Aalto University
School of Chemical
Technology

School of Chemical Technology
Degree Programme of Chemical Technology

Laura Suominen

IMPURITY REMOVAL OF VACUUM GAS OIL

Master's thesis for the degree of Master of Science in Technology submitted for inspection, Espoo, 22 May, 2016.

Supervisor **Professor Pekka Oinas**

Instructors **D. Sc. (Tech.) Aarne Sundberg**
D. Sc. (Tech.) Sarwar Golam

Aalto University
School of Chemical
Technology

Aalto University, P.O. BOX 11000, 00076 AALTO
www.aalto.fi

Abstract of master's thesis

Author Laura Suominen

Title of thesis Impurity removal of vacuum gas oil

Department Department of Biotechnology and Chemical Technology

Professorship Plant Design **Code of professorship** KE-107

Thesis supervisor Professor Pekka Oinas

Thesis advisors/Thesis examiners D. Sc. (Tech.) Aarne Sundberg, D. Sc. (Tech.) Sarwar Golam

Date 22.5.2016 **Number of pages** 107+1 **Language** English

Abstract

Generally, vacuum gas oil (VGO) is defined as a petroleum distillate boiling between 350 and 550 °C at 1 atm. VGO is produced from atmospheric residue in a vacuum distillation unit. The amount and nature of impurities in VGO depend greatly on the origin of the crude oil but the distillation range of the petroleum cut also affects the impurity level. Typical impurities are nitrogen, sulphur and metals such as nickel, vanadium and iron.

As crude oil typically has a large excess of heavy cuts and an insufficient amount of light cuts and middle distillates, the heaviest cuts need to be converted into lighter products. Before VGO is converted into more valuable lighter products, it is fed to a catalytic hydrodesulphurization (HDS) process to reduce the sulphur levels. However, the impurities present in VGO lead to deactivation of HDS catalyst. Therefore, an effective impurity removal method prior to HDS process would extend the catalyst lifetime and reduce refinery downtime.

The impurity removal methods discussed in this thesis are solvent deasphalting, demetallization by acids, phosphorous compounds and supercritical water, and photochemical denitrogenation and desulphurization. Based on the advantages and disadvantages of the methods, demetallization using phosphorous compounds was chosen to be preliminarily designed in the applied part of the thesis.

The VGO feed contained 10 ppm of metal impurities. When no demetallization pretreatment was applied, the HDS catalyst lifetime was only 8 weeks. In the demetallization process phosphoric acid was used as the phosphorous compound. The acid was mixed with the VGO in a static mixer and the phases were separated in three parallel decanters. Phosphoric acid reduced the concentration of Ni, V and Fe and the removal rates used in the calculations were 32 w%, 23 w% and 22 w%, respectively. As a result, the HDS catalyst lifetime was 9 weeks. The catalyst lifetime was extended only by one week and the demetallization process was not profitable with current costs.

Keywords vacuum gas oil, VGO, impurity removal, hydrodesulphurization, HDS, demetallization, phosphoric acid

Aalto-yliopisto
Kemian tekniikan korkeakoulu

Aalto-yliopisto, PL 11000, 00076 AALTO
www.aalto.fi

Diplomityön tiivistelmä

Tekijä Laura Suominen		
Työn nimi Tyhjökaasuöljyn epäpuhtauksien poisto		
Laitos Biotekniikan ja kemian tekniikan laitos		
Professuuri Tehdassuunnittelu		**Professuurikoodi** KE-107
Työn valvoja Professori Pekka Oinas		
Työn ohjaajat/Työn tarkastajat TkT Aarne Sundberg, TkT Sarwar Golam		
Päivämäärä 22.5.2016	**Sivumäärä** 107+1	**Kieli** Englanti

Tiivistelmä

Yleisesti tyhjökaasuöljy (*vacuum gas oil*, VGO) määritellään raakaöljyjakeeksi, joka tislautuu ilmanpaineessa 350–550 °C:n lämpötilassa. Se valmistetaan tyhjötislaamalla pohjaöljystä. VGO:n sisältämien epäpuhtauksien määrä ja laatu riippuu suuresti raakaöljyn alkuperästä, mutta myös jakeen tislausväli vaikuttaa epäpuhtaustasoon. Tyypillisiä epäpuhtauksia ovat typpi, rikki ja metallit, kuten nikkeli, vanadiini ja rauta.

Koska raakaöljy tyypillisesti sisältää liikaa raskaita jakeita ja riittämättömästi kevyitä jakeita ja keskitisleitä, raskaimmat jakeet jalostetaan kevyemmiksi tuotteiksi. Ennen tätä VGO:n sisältämä rikki poistetaan katalyyttisesti vedyn avulla (*hydrodesulphurization*, HDS). VGO:n sisältämät epäpuhtaudet kuitenkin deaktivoivat rikinpoistossa käytetyn katalyytin. Tästä johtuen tehokas epäpuhtauksien poistomenetelmä ennen rikinpoistoprosessia pidentäisi katalyytin elinikää ja vähentäisi seisokkien tarvetta.

Tässä työssä käsiteltyjä epäpuhtauksien poistomenetelmiä ovat deasfaltointi, metallinpoisto happojen, fosforiyhdisteiden ja ylikriittisen veden avulla sekä fotokemiallinen typen- ja rikinpoisto. Menetelmien etujen ja haittojen perusteella esisuunnitteluun valittiin metallinpoisto fosforiyhdisteiden avulla. Prosessin esisuunnittelu toteutettiin työn soveltavassa osassa.

VGO-syöttö sisälsi 10 ppm metalliepäpuhtauksia. Kun metallinpoistoa ei ollut, rikinpoistokatalyytin elinikä oli ainoastaan 8 viikkoa. Metallinpoistoprosessissa fosforiyhdisteenä käytettiin fosforihappoa. Happo sekoitettiin VGO-virtaan staattisessa sekoittimessa ja faasit erotettiin toisistaan kolmessa rinnakkaisessa dekantterissa. Fosforihappo vähensi nikkelin, vanadiinin ja raudan pitoisuutta ja laskuissa käytetyt poistoprosentit olivat nikkelille 32 m-%, vanadiinille 23 m-% ja raudalle 22 m-%. Tämän seurauksena rikinpoistokatalyytin elinikä oli 9 viikkoa. Katalyytin elinikä piteni vain yhdellä viikolla eikä metallinpoistoprosessi ollut kannattava nykyisillä kustannuksilla.

Avainsanat tyhjökaasuöljy, VGO, epäpuhtauksien poisto, rikinpoisto vedyllä, HDS, metallinpoisto, fosforihappo

Preface

This master's thesis was conducted for Neste in the Technology Centre of Porvoo refinery between October 2015 and March 2016. The thesis was supervised by professor Pekka Oinas from Aalto University.

I would like to thank my advisors D. Sc. (Tech.) Aarne Sundberg and D. Sc. (Tech.) Sarwar Golam for the guidance they gave me during my work. I would also like to thank Jaana Makkonen who was responsible of the project for which my thesis was done. She offered help and encouraging comments throughout the process. Furthermore, I wish to thank Prof. Pekka Oinas for reviewing my thesis and giving me valuable advice.

Finally, I want to thank my family and friends. I am thankful for the support and encouragement of my family and for all the great moments with my friends that made my time in Otaniemi so memorable.

Porvoo, March 24th, 2016

Laura Suominen

Table of Contents

Abbreviations

ASME	American Society of Mechanical Engineers
BPVC	Boiler & Pressure Vessel Code
CEPCI	Chemical Engineering Plant Cost Index
DAO	Deasphalted oil
HDS	Hydrodesulphurization
LHSV	Liquid Hourly Space Velocity
NFPA	National Fire Protection Association
NPV	Net present value
PDMS	Polydimethylsiloxane
SCW	Supercritical water
SDA	Solvent deasphalting
TAN	Total acid number
VGO	Vacuum gas oil

1 Introduction

Importance of upgrading heavy oils is increasing as heavier crudes are more often utilized to meet the demand of lighter oils. Heavy oils contain significant quantities of metal, sulphur and nitrogen contaminants which complicate the upgrading process. The metals, mainly vanadium and nickel, pose a particular problem for refineries as they accumulate on catalysts causing permanent deactivation. (Mandal *et al*., 2012)

Sulphur contaminants present in petroleum can be removed in a catalytic hydrodesulphurization (HDS) process. Although the process is capable of selectively removing the contaminants, a major drawback is the formation of metal deposits on the catalyst. Therefore, a guard bed consisting of a cheaper hydrogenation catalyst is used to prevent the deactivation of desulphurization catalyst. Due to the fast deactivation of the guard bed catalyst, it needs to be changed regularly to maintain the activity. (Fahim *et al*., 2010)

Alternative impurity removal methods have been used and studied (Ali & Abbas, 2006). By removing the contaminants in a pretreatment process before desulphurization, the formation of deposits on the catalyst surface would decrease. As a result, the catalyst deactivation would be reduced and the heavier petroleum fractions with high impurity levels could be more cost-efficiently upgraded.

1.1 Goals of the thesis

The aim of this thesis was to study possible impurity removal methods for vacuum gas oil prior to the hydrodesulphurization process. An impurity removal pretreatment could enable the use of cheaper, poor-quality vacuum gas oil which has high impurity levels. By decreasing the impurity levels, the catalyst lifetime could be extended as without any pretreatment, the catalyst would be rapidly deactivated by the high amount of

impurities. As a result, the catalyst could be replaced less frequently reducing refinery downtime and leading to significant financial savings.

1.2 Scope of the thesis

In the literature part of this thesis, the most common impurities present in the vacuum gas oil are presented and their effects are discussed. Different impurity removal methods were studied excluding adsorbent materials and guard beds. Comparison of the methods was conducted and based on their advantages and disadvantages, one of the impurity removal processes was chosen for prestudy. The prestudy was carried out in the applied part of the thesis and includes preliminary design and sizing of process equipment, cost estimation and discussion about safety. In addition, the HDS process with the impurity removal was compared to the HDS process without any pretreatment and a sensitivity analysis was conducted.

LITERATURE PART

2 Vacuum gas oil

Vacuum gas oil (VGO) is a petroleum distillate boiling between 350 and 550 °C at 1 atm (Leprince, 2001; Toulhoat & Raybaud, 2013). It is produced from atmospheric residue in a vacuum distillation unit. VGO is further processed to produce light and middle distillates. (Parkash, 2003) A flow scheme of crude oil refining is presented in Figure 1 where vacuum distillation can be seen in relation to other refinery units.

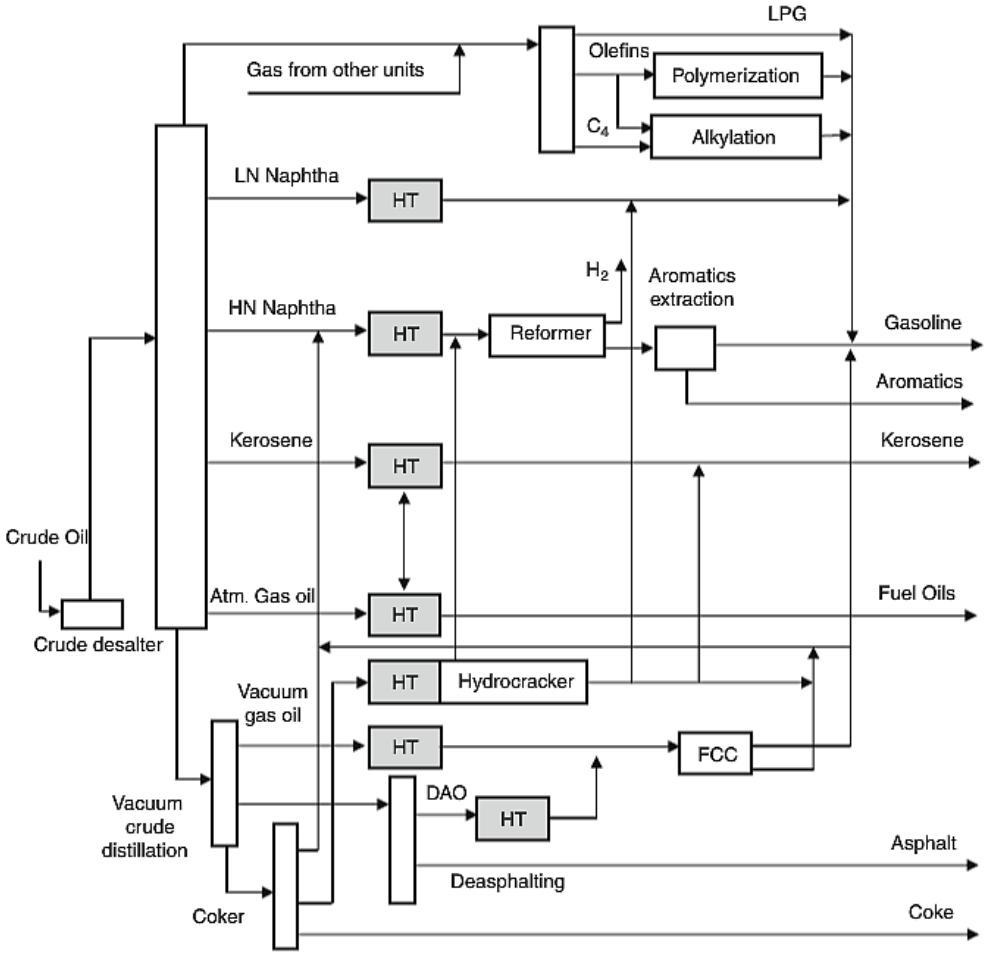

Figure 1. Oil refinery flow scheme (Fahim *et al*., 2010).

Crude oil entering a refinery is first distilled in an atmospheric distillation tower in order to fractionate the hydrocarbons. Due to the fragility of some molecules which start to crack at around 380-400 °C, the atmospheric distillation can fractionate hydrocarbons with boiling point below 350-380 °C. Distilling heavier fractions from crude oil is impossible at atmospheric pressure. Therefore, distillation is continued under vacuum to stay within the temperature range that the compounds can withstand. (Marcilly, 2006)

The heaviest cut distilling above 350-380 °C forms the atmospheric residue which is used as the feed to the vacuum distillation. In a vacuum distillation tower, the atmospheric residue is fractionated into vacuum gas oil and vacuum residue. (Marcilly, 2006; Fahim *et al.*, 2010) The vacuum is produced by steam ejectors taking suction from the top of the distillation tower. The pressure at the top of the tower is 0.4-0.7 kPa and in the flash zone about 3-4 kPa. (Jones & Pujadó, 2006) Boiling ranges of VGO and vacuum residue in relation to other petroleum cuts are shown in Figure 2.

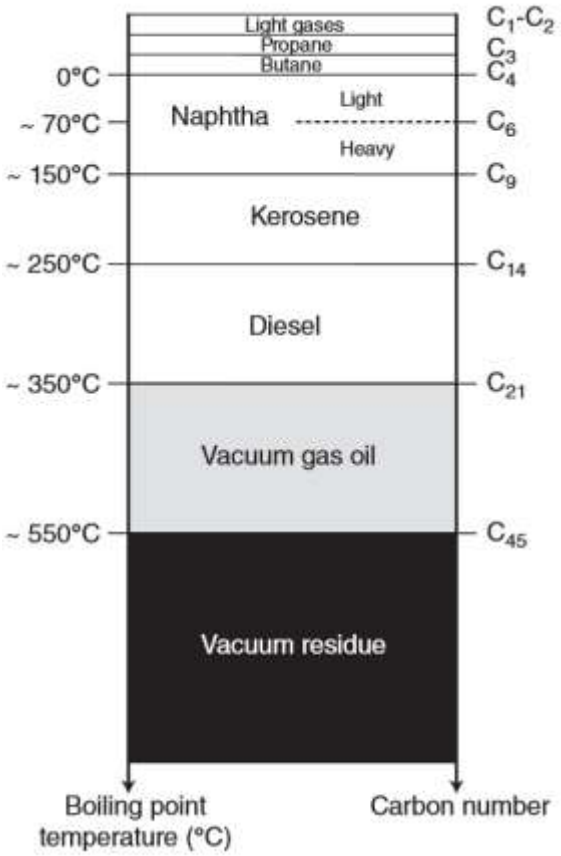

Figure 2. Different petroleum cuts with their boiling range and carbon number (Toulhoat & Raybaud, 2013).

However, these distillation cuts of crude oil do not correspond to the market demand of petroleum products. Crude oil has typically a large excess of heavy cuts and an insufficient amount of light cuts and middle distillates. To adjust these quantities, the heaviest cuts need to be converted into lighter products which are in high demand. To improve the product quality to meet the applicable specifications, some cuts have to undergo purification treatment and/or restructuring of the molecules. (Marcilly, 2006)

Most crude oils contain traces of different metal complexes. These impurities concentrate in the residue and therefore, VGO contains several impurities. Nickel and vanadium are the most abundant and troublesome metal complexes present in the

organic parts of fossil fuels deposits. Even though present only in trace quantities, they lead to deactivation of both desulphurization and cracking catalysts. (Dechaine & Gray, 2010) To prevent the deactivation of the catalysts, various methods for pretreating VGO have been studied and are presented in chapter 4.

3 Impurities in VGO

The amount and nature of impurities in VGO depend greatly on the origin of the crude oil. The distillation range of the petroleum cut also affects the impurity level. Typical impurities are nitrogen, sulphur and metals such as nickel, vanadium and iron. (Leprince, 2001) Typical VGO impurity composition is presented in Table 1.

Table 1. Typical VGO impurity composition (Toulhoat & Raybaud, 2013).

Impurity	Unit	VGO
Sulphur	wt %	0.1–2
Nitrogen	wt ppm	300–2000
Basic nitrogen	wt ppm	440
Nickel	wt ppm	< 0.5
Vanadium	wt ppm	< 0.5
Asphaltenes	wt ppm	< 100

In this chapter, different impurities and their harmful effects are discussed. The impurities presented are nitrogen, sulphur, asphaltenes, vanadium, nickel, carbon residue, iron, calcium and silicon.

3.1 Nitrogen

Vacuum gas oil contains different types of nitrogen compounds such as anilines, compounds containing a five-atom ring (indoles and carbazoles) and compounds containing a six-atom ring (quinolines and acridines). Nitrogen is predominantly present in these heterocyclic N-rings. The five- and six-membered N-rings are classified as non-basic and basic nitrogen compounds, respectively. The non-basic N-rings are based on a pyrrole core and the basic ones on a pyridine core. (Macaud *et al*., 2004; Furimsky & Massoth, 2005) The pyridines are less reactive than pyrroles but they have a stronger tendency to adsorb on the catalyst (Leprince, 2001). The structures of different nitrogen compounds are presented in Figure 3.

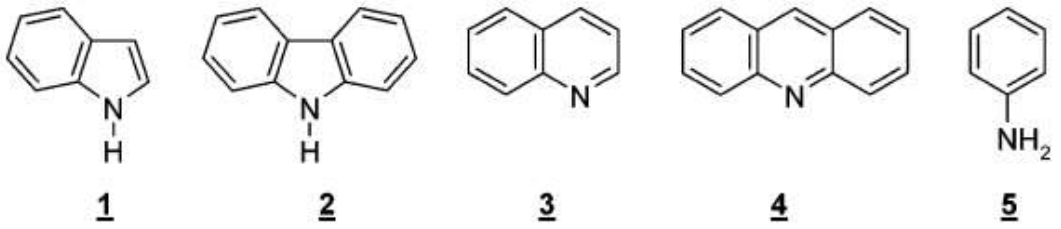

Figure 3. Nitrogen compounds in petroleum: 1 indole, 2 carbazole, 3 quinoline, 4 acridine and 5 aniline (Macaud *et al*., 2004).

For hydroprocessing, nitrogen compounds are the most common catalyst poisons due to their strong adsorption on catalyst sites. They adsorb on catalyst acidic sites: Lewis and Brønsted sites. Adsorbing on Lewis sites occurs via the N-electron pair or via the aromatic π-system and on Brønsted sites by interacting with protons. The adsorption can be reversible or irreversible, depending on reaction conditions. (Furimsky & Massoth, 1999)

The basic nitrogen compounds act as strong inhibitors towards the hydrodesulphurization (HDS) reaction as they poison the acidic sites of the catalysts. Besides poisoning the hydroprocessing catalysts, the nitrogen compounds are precursors of coke formation. Sau *et al.* (2005) studied the inhibiting effect of nitrogen compounds in crude oil on hydrotreating and hydrocracking reactions. Their results showed that the inhibitive effects of nitrogen on hydrocracking conversion are highly non-linear and the conversion rapidly drops as the nitrogen level increases. At higher reaction temperature, the drop in activity or conversion is less than in lower temperatures. This is a result of the higher rate of desorption of nitrogen compounds at elevated reaction temperatures. Selective removal of nitrogen would both increase significantly the activity of hydrodesulphurization catalyst and reduce the hydrogen consumption. (Sau *et al*., 2005)

As the 5-membered N-rings are less resistant to hydrogenation compared to the 6-membered rings, the relative contribution of 5-membered rings to poisoning was expected to be less important. Therefore, many authors have used pyridine as a poison in HDS studies. (Furimsky & Massoth, 1999) However, Laredo *et al.* (2001) studied the inhibition effect of non-basic nitrogen compounds on HDS of dibenzothiophene. They discovered that the inhibitive effect of indole and carbazole was comparable to that of quinoline. The inhibiting effect of these three compounds was very strong even with as low nitrogen concentrations as 5 ppm. A mixture of indole, carbazole, and quinoline was found to have a stronger inhibiting effect than any of the individual components at equivalent concentrations. (Laredo *et al*., 2001)

3.2 Sulphur

The amount of sulphur present is strongly correlated with the density of the oil cuts. Therefore, the most of the sulphur compounds are in the heavier cuts. Sulphur is present as thiols, sulphides, disulphides, sulphoxides, and thiophenes. In heavy fractions, main sulphur compounds are thiophenes, followed by cyclic and acyclic sulphide derivatives.

Sulphoxides are present only in small amounts. (Bertoncini *et al*., 2013) The structures of common sulphur compounds are shown in Figure 4.

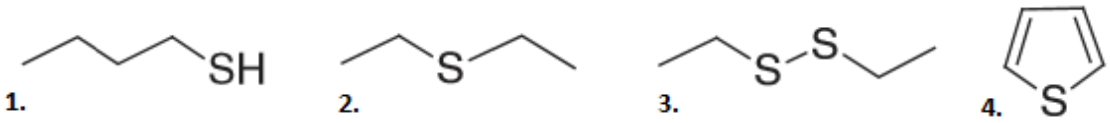

Figure 4. Structures of sulphur compounds present in VGO: 1. thiol, 2. sulphide, 3. disulphide, and 4. thiophene (Bertoncini *et al*., 2013).

Sulphur compounds are poisons for noble metal catalysts and in fuels lead to atmospheric pollutants such as SO_2 (Bertoncini *et al*., 2013). Sulphur oxide gases react with water in the atmosphere causing acid rain which damages buildings and acidifies soil. Sulphur emissions also cause respiratory illnesses and contribute to formation of atmospheric particulates. (Srivastava, 2012) In addition, the presence of sulphur is undesirable for the reasons of corrosion, bad odor and poor burning. Products containing high amount of sulphur have low heating values and are considered of poor quality. (Riazi, 2005)

Environmental regulations are imposing strict limits for sulphur levels in transportation fuels. Currently, the maximum sulphur content allowed in petrol and diesel in the European Union is 10 mg/kg. (European Parliament & Council of the European Union, 2009)

3.3 Asphaltenes

Asphaltenes are generally described as n-heptane insoluble components (Gawel *et al*., 2005). They are the most complex and biggest molecules in petroleum (Sun *et al*., 2010). Asphaltenes consist of condensed polynuclear aromatic layers linked by saturated

chains. Their molecular weights vary from a few hundred to several million and they contain various heteroatoms, such as sulphur, nitrogen, and metals. (Fahim *et al*., 2010)

Asphaltenes cause problems in the processing of VGO. During hydroprocessing, they undergo various reactions involving both cracking and hydrogenation which change their structure. Asphaltenes are the predominant cause of deposit formation. They function as coke precursors that lead to catalyst deactivation in hydroprocessing. In addition, the metals present in heavy feedstocks are mainly located in asphaltenes. Therefore, catalyst deactivation results from the accumulation of both carbonaceous and metallic deposition. Asphaltenes have a high tendency to adsorb onto the catalyst surface blocking the pores and preventing other molecules from accessing the active sites. (Gawel *et al*., 2005) The effects of metals are discussed in more detail later in this chapter.

The asphaltene quality is more important than the quantity in coke deposition. For example, the increase in aromaticity causes higher coke yield. Also increasing the content of polar components increases the amount of coke deposition. (Gawel *et al*., 2005)

3.4 Nickel and vanadium

The most abundant metals are nickel and vanadium. Nickel and vanadium are present in the form of oil-soluble organometallic complexes. The most common are of porphyrin type with a nickel or vanadium atom bonded to nitrogen atoms with four heterocyclic structures. (Speight, 1999; Leprince, 2001) In petroleum, nickel occurs in the +2 valence state while most vanadium atoms have a valence of +4, almost exclusively as vanadium ions VO^{2+}. Examples of a nickel and a vanadyl porphyrin complex are presented in Figure 5. Metals are also present in non-porphyrin structures which are not as extensively studied as the porphyrin structures. (Mandal *et al*., 2014)

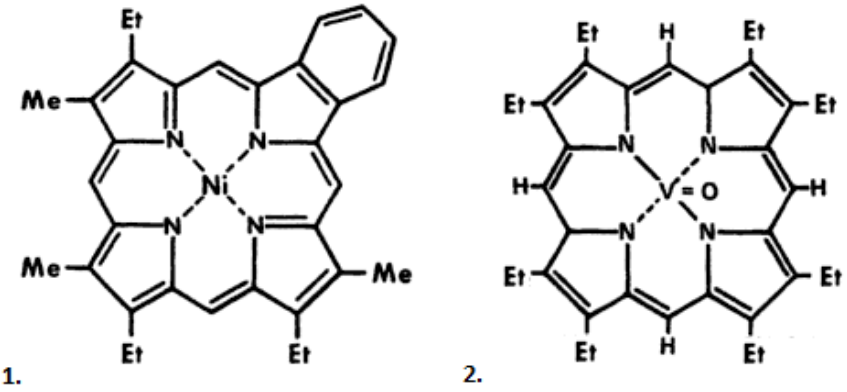

Figure 5. Structures of two porphyrins: 1. benzoporphyrin and 2. vanadyl octaethylporphyrin (Speight, 1999).

As the metals accumulate on the catalyst surface, they start to plug up the catalyst pores leading to catalyst deactivation. The accumulation of metals reduces the access to the active sites dispersed in the pores of the catalyst. Metals are deposited in the form of metal sulphides such as Ni_3S_2 and VS_2. They will mainly be deposited in the outer shell of the catalyst particles so the pore plugging occurs even at relatively low levels of metal deposition. (Toulhoat & Raybaud, 2013) The metal sulphides gradually narrow the pores and in order to maintain the design activity, temperature is raised to offset the deactivation of the catalyst. However, at some point either the temperature is too high for the reactor design or the loss of active sites by pore plugging is too large to maintain the design activity by raising the temperature. (Furimsky & Massoth, 1999)

The deactivation by metals is irreversible and it always occurs simultaneously along with the deactivation by coke. The initial deposition occurs at higher rate for vanadium than for nickel and increases with larger pore diameter. Therefore, the formation of vanadium deposits may have an adverse effect on the rate of nickel deposit formation. (Furimsky & Massoth, 1999) In addition, both nickel and vanadium exhibit dehydrogenation

activity. Their presence on the catalyst promotes dehydrogenation reactions during a cracking process which results in increased amounts of coke and light gases at the expense of gasoline production. (Ali & Abbas, 2006)

3.5 Carbon residue

Carbon residue is formed by evaporation and thermal degradation of a carbon-containing material (Rand, 2010). Carbon residue consists of the nonvolatile carbonaceous compounds of a petroleum fraction when vaporized in the absence of air at atmospheric pressure. The heavier fractions with more aromatics have higher carbon residues than light and volatile fractions. (Riazi, 2005)

Higher carbon residue values indicate low-quality fuel and lower hydrogen content. Moreover, carbon residue increases when sulphur, nitrogen or asphaltenes content or the viscosity of the oil increases. When hydrogen content increases, the carbon residue decreases. (Riazi, 2005)

The residue is not composed entirely of carbon. It is coke that can be further processed by carbon pyrolysis. (Rand, 2010) Coke is one of the main reasons for the deactivation of hydrotreatment catalysts. Particularly, it leads to plugging which can cause significant losses of the initial surface area. Coke consists of a deposit of hydrocarbons which agglomerate to form a film of varying thickness on the surface of a catalyst. (Toulhoat & Raybaud, 2013)

In petroleum hydrotreatment processes, catalyst deactivation by coke and metal deposits occurs simultaneously. As can be seen in Figure 6, coke deposits rapidly during the initial stages before reaching a steady-state. Concurrently, metals exhibit relatively linear deposition patterns with time. (Furimsky & Massoth, 1999; Toulhoat & Raybaud, 2013)

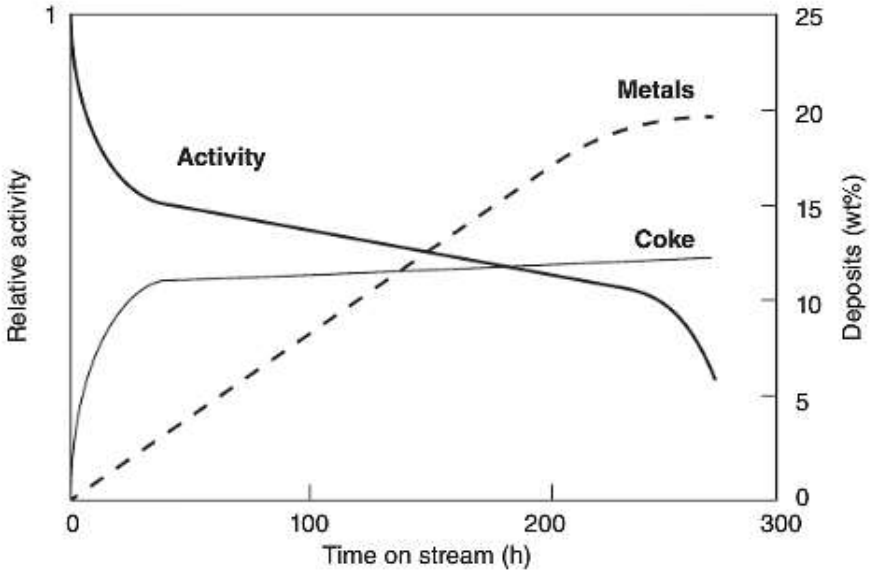

Figure 6. Coke and metal concentrations and the catalyst activity evolution in residue hydrotreatment (Toulhoat & Raybaud, 2013).

The coke build-up increases with molecular weight and boiling range of the feed. The main reactions leading to coke formation are polymerization and polycondensation. Among the hydrocarbon groups, alkenes, aromatics and heterocyclics are the most susceptible to coke formation. They are more likely to convert to higher molecular weight compounds than the saturated hydrocarbons. (Furimsky & Massoth, 1999)

3.6 Iron

Iron compounds present in VGO originate not only from the crude oil but also from corrosion. Similarly to nickel and vanadium, iron is present in the structures of porphyrin compounds. In addition to that, iron is complexed as iron naphthenate. Under hydrotreating conditions, these complexes are decomposed on the catalyst surface due to the reaction with hydrogen. Thus, iron is deposited in the form of iron sulphide in the

catalyst pores. (Leprince, 2001) The results of iron deposits are the blocking of active sites and loss of porosity (Furimsky & Massoth, 1999).

Present in crude oils, naphthenic acids are saturated cyclic compounds containing one or more carboxyl groups. These acids are corrosive to carbon and low alloy steels, stainless steels and some nickel alloys at temperature range of 220-420 °C. The presence of hydrogen sulphide affects the corrosion mechanisms and the following reactions (1-3) are observed to compete with each other. The last reaction regenerates naphthenic acid and therefore causes further corrosion. (Ropital, 2009)

Direct acid attack on iron: $\mathrm{Fe} + 2\mathrm{RCOOH} \leftrightarrow \mathrm{Fe(RCOO)_2} + \mathrm{H_2}$ (1)

Corrosion due to hydrogen sulphide: $\mathrm{Fe} + \mathrm{H_2S} \leftrightarrow \mathrm{FeS} + \mathrm{H_2}$ (2)

Attack of iron naphthenate by H_2S: $\mathrm{Fe(RCOO)_2} + \mathrm{H_2S} \leftrightarrow \mathrm{FeS} + 2\mathrm{RCOOH}$ (3)

Petroleum fractions with TAN (Total Acid Number) greater than 1.5 are potentially corrosive. Besides the TAN, the type of acid and the presence of H_2S are important parameters. For naphthenic acids with high molecular weight, the steric hindrance due to their long carbon chain would slow the formation of iron naphthenates and hence the corrosion rate. To prevent the corrosion, steels with increasing chromium and molybdenum contents offer enhanced corrosion resistance. (Ropital, 2009)

3.7 Calcium

Calcium is usually present in combination with naphthenic acid as soaps (Ali & Abbas, 2006). Offshore crude oil production installations around the world are associated with the precipitation of calcium naphthenate soaps. The soaps result from the interaction of polycyclic tetracarboxyl acids with divalent calcium ions (Ca^{2+}) present in produced waters. These tetraprotic naphthenic acids are known as ARN acids. Due to the four reactive carboxylate groups within each molecule, the ARN acids are cross-linked by

calcium ions to form long polymeric networks. The calcium naphthenate soaps are insoluble in both crude oil and water. (Juyal *et al*., 2015)

The precipitation of calcium naphthenate soaps causes significant operational challenges. Calcium naphthenate scale is one of the most challenging depositions in crude oil production. The deposits occur as viscous, sticky solids and sludges that harden upon exposure to air causing physical blockages in production facilities, for example in oil-water separators, desalters, heat exchangers and pipelines. Moreover, the deposits need to be physically removed which increases maintenance costs and possibly leads to replacement of production equipment. (Juyal *et al*., 2015)

3.8 Silicon

In petroleum products, the presence of silicon is mainly due to the use of antifoaming agents such as polydimethylsiloxanes (PDMS). The antifoaming agents are used to enhance the crude oil recovery from the reservoir and to avoid the formation of emulsions in refinery processes. PDMS degrades around 300 °C generating various different silicon degradation products, such as siloxanes, silanes and silanols, which can then react with the hydrocarbon matrix. (Chainet *et al*., 2011; Chainet *et al*., 2013)

By adsorbing on catalyst surface, silicon acts as a catalyst poison causing deactivation. However, silicon species have different effects on the catalytic process depending on the nature of the catalyst, on the experimental conditions and especially on the chemical nature of the silicon molecule. Due to the instability of several silicones, the reactivity and the chemical nature of the silicon compounds are unknown which complicate the understanding of silicon poisoning. (Chainet *et al*., 2011; Chainet *et al*., 2013)

4 Impurity removal methods

The aim of this thesis is to study impurity removal methods preceding sulphur removal unit to decrease the deactivation of desulphurization catalyst. Therefore, the process for removing sulphur is not discussed. The impurity removal methods presented are divided into physical and chemical methods.

Metal deposition on hydrotreatment catalysts is irreversible and there is no possibility of recovering the initial catalytic activity of the catalysts. The pore plugging caused by metal deposits cannot be removed which sets a limit to the activity recovery. (Toulhoat & Raybaud, 2013) Thus, finding an effective metal removal method would extend the catalyst lifetime and enable better activity recovery.

4.1 Physical method

The physical method discussed is an extraction treatment called solvent deasphalting. An advantage of the solvent deasphalting is that the extraction can be performed under moderate operating conditions. However, finding a solvent that is sufficiently selective can be problematic. It is reported that extraction treatment leads to a loss of 5-15 wt% of the initial amount of saturated hydrocarbons. (Gaile *et al*., 2001)

4.1.1 Solvent deasphalting

Solvent deasphalting (SDA) is a separation process in which the residue is separated by molecular weight instead of by boiling point. In the SDA process, heavy feedstock is separated into deasphalted oil (DAO) with low metal content and a heavy pitch stream containing most of the contaminants. The feed is mixed with a light paraffinic solvent, typically C_3-C_7. Due to their insolubility to these solvents, asphaltenes will precipitate out of the mixed feedstock. (Fahim *et al*., 2010) An advantage of SDA extraction is that it can

be operated in relatively low temperature and pressure conditions (Lee *et al*., 2014). However, the process removes convertible material along with the metal-containing species (Mandal *et al*., 2014).

As the metals, sulphur and nitrogen are mainly concentrated in the heavier molecules of petroleum, their content in DAO is significantly reduced (Parkash, 2003). This can be seen in Figure 7 where vacuum residue was used as a feed to SDA process.

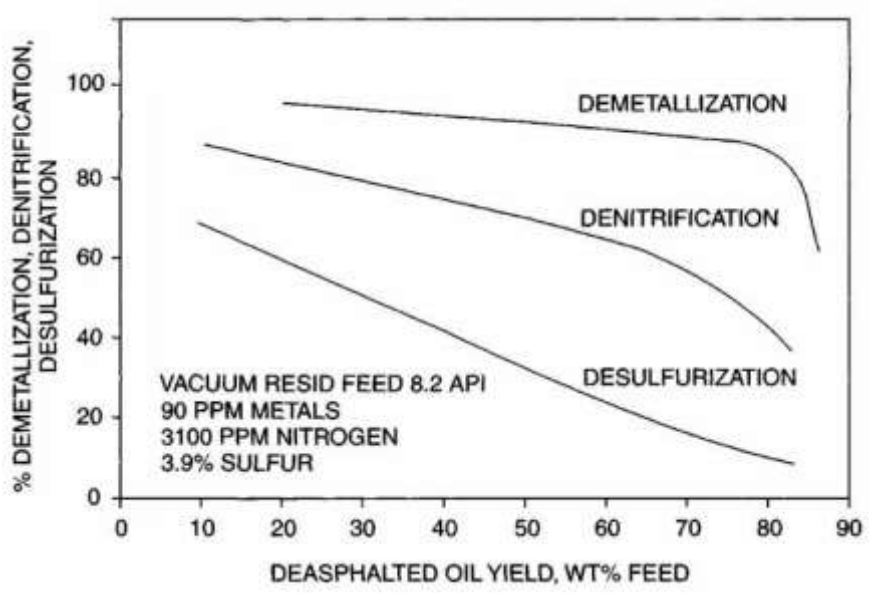

Figure 7. Percent of demetallization, denitrification and desulphurization as a function of DAO yield (Parkash, 2003).

The SDA process consists of extraction, DAO recovery, asphalt recovery and solvent recycling system (Parkash, 2003). A process flow chart is presented in Figure 8. Due to its high viscosity, the feed is mixed with a small amount of solvent prior to the extraction tower. The feed, with a relatively small amount of solvent, enters the extraction tower at a point about two-thirds up the column while the solvent enters near the bottom of the tower. The extraction tower is a multistage contactor equipped with, for example,

baffle trays or rotating discs. In the tower, the heavy oil flows downward as the light solvent goes upward. Asphalt is insoluble in the solvent and therefore, it precipitates and flows towards the bottom of the tower. (McKetta, 1992; Parkash, 2003)

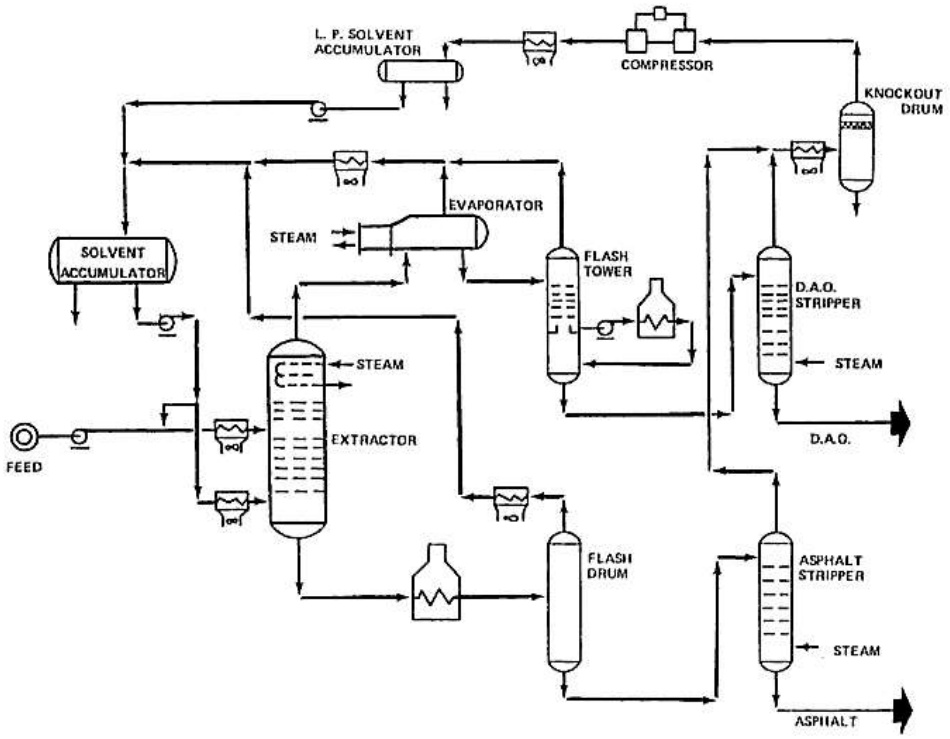

Figure 8. Process flow chart of a SDA process (McKetta, 1992).

The separation of the asphalt from the oil is controlled by varying the solvent/oil ratio and by maintaining a temperature gradient across the extraction tower. The highest temperature is at the top of the tower and the lowest at the solvent inlet. Steam is used in the heating coils in the top of the tower to regulate the temperature. The steam flow is adjusted to the feed inlet temperature. (McKetta, 1992)

The dissolved DAO leaves the top of the tower and flows to an evaporator where vaporized solvent is separated from the DAO. The liquid flows from the bottom of the

evaporator to a flash tower where most of the remaining solvent is vaporized. Finally, the DAO is fed to a steam stripper operating at atmospheric pressure. Superheated steam enters the lower part of the tower. The remaining solvent is stripped out and flows overhead with the steam through a condenser into a compressor suction drum where the water is removed. The DAO product is obtained from the stripper bottom. (McKetta, 1992)

The asphalt and solvent mixture obtained from the bottom of the extraction tower flows through a heater into a flash drum. In the flash drum, the vaporized solvent is separated from the asphalt. Asphalt, with a small quantity of solvent, flows from the bottom of the flash drum to an asphalt steam stripper. The steam and solvent vapors leave from the top of the stripper and are mixed with the DAO stripper overhead. Solvents recovered from each of the process steps are recycled into solvent accumulators and can be reused. (McKetta, 1992) The asphaltene-rich pitch can be utilized to produce heat and hydrogen by gasification and as a road-packing material (Lee *et al*., 2014).

The selection of a solvent significantly affects the performance, flexibility and economics of the process. The solvent must be suitable for the extraction of desired oil fraction and for the control of the yield and/or the quality of the DAO at temperatures which are within the practical operating limits. (McKetta, 1992) Selectivity is the ability of the solvent to separate the paraffinic and possibly resinous oils from the asphalt. The selectivity can be improved by increasing the solvent/oil ratio at a constant DAO field. However, there is always an optimum solvent/oil ratio for each operation due to the energy consumption in the recovering of the solvent. (Parkash, 2003) Increasing the carbon number of the solvent reduces the quality of the DAO but enhances the yield of DAO produced because hydrocarbons of higher molecular weight become soluble in the solvent (Lee *et al*., 2014).

If the operating temperature approaches the critical temperature of the solvent, the process becomes unstable. For example, the critical temperature of propane is 97 °C

which limits the extraction temperature to about 80 °C. Generally, the greater the temperature difference between the top and the bottom of the extraction tower, the better will be the quality of the DAO. This results from the internal reflux that is generated in the tower. However, too much internal reflux can cause flooding. The extraction tower pressure must be higher than the vapor pressure of the solvent at the tower operating temperature. (McKetta, 1992)

4.2 Chemical methods

In this chapter, chemical methods including demetallization processes using acids, phosphorous compounds and supercritical water are discussed. Also a photochemical denitrogenation and desulphurization process is presented. Instead of chapter 4.2.1, the metal removal methods utilizing phosphorous and phosphoric acids are discussed in chapter 4.2.2 among the other phosphorous compounds.

4.2.1 Demetallization by acids

Generally in a demetallization process with an acid, the metal compounds are converted into water-soluble constituents or to constituents separable in aqueous phase from the oil phase (Powell, 1957). The demetallization of oil-soluble metalloporphyrins (MP) by acids (HX) is a reversible reaction which can be presented by the following equation (Ali & Abbas, 2006):

$$\mathrm{MP} + \mathrm{HX} \leftrightarrow \mathrm{PH} + \mathrm{MX} \tag{4}$$

Abbas *et al.* (2010) treated heavy furnace oil with various chemicals to remove nickel and vanadium. Among the acids used in the experiments, sulphuric acid showed the most promising results. (Abbas *et al*., 2010) Moreover, treatment of petroleum fractions with sulphuric acid to improve the quality has been used commercially for many years. In the treatment with sulphuric acid, some of the acid is almost always reduced to sulphur

dioxide. Consequently, sulphur dioxide may react with unsaturated hydrocarbons forming additional products such as sulphones, polysulphones and aromatic sulphonic acids. It is a disadvantage that sulphuric acid reacts with and promotes reactions of hydrocarbons. (Ali & Abbas, 2006) Another problem in the demetallization process is the possible formation of a stable emulsion. The more viscous the oil is the more readily it emulsifies with the acid. (Abbas *et al*., 2010)

Powell (1957) patented a process for the removal of heavy metals with sulphuric acid. The process was designed to be prior to a catalytic cracking operation. The sulphuric acid used in the demetallization had a concentration of 10 % acid. After the oil was mixed with the dilute sulphuric acid, it was washed with water in order to transfer the acidified metal components from the oil to the aqueous phase. If no difficult emulsions were formed, the mixture could be settled to effect the separation of oil and aqueous phases. In cases where difficult emulsions were produced, the mixture was neutralized with an alkaline agent to a pH value within 6.5-7.5 before the separation of the aqueous phase from the oil phase. Another option to resolve the emulsion was to use electrical precipitation. (Powell, 1957)

Kimberlin Jr. and Judson (1959) patented a technique also utilizing sulphuric acid for the removal of nickel, vanadium and iron contaminants from heavy gas oil before catalytic cracking process. Sulphuric acid reacted with the contaminants to form acid sludge which could be separated from the oil phase by settling/decantation. The optimal processing temperature was 93 °C at atmospheric pressure with the sulphuric acid concentration of 80 %. Higher temperatures resulted in lower oil yields with high acid consumption due to the occurrence of oxidation reactions. (Kimberlin Jr. & Judson, 1959)

Various different acids have been studied and patented for the removal of organically-bound calcium compounds from hydrocarbonaceous feedstocks. Kuehne *et al.* (2005) patented a method where the calcium-containing hydrocarbonaceous feedstock was treated with aqueous extraction solution consisting of acetate ion and alkaline material

at the pH range of 3.0-5.0. Acetic acid was a suitable source of acetate ions and, for example, ammonium hydroxide, sodium hydroxide and potassium hydroxide were possible alkaline materials. While the alkaline material was added to keep the pH value within the particular range, the acetate ions of the solution formed water-soluble complexes with calcium. (Kuehne *et al*., 2005)

According to the patent, acetate ion at the specific pH facilitated the decomposition of calcium compounds and provided a mechanism for more easily transporting the calcium ions from the oil phase to the aqueous phase. Surprisingly high calcium removal in the pH range between 3.0 and 5.0 was related to the pH at which organically-bound calcium was most easily dissociated. The calcium removal as a function of the pH value is presented in Figure 9. The pH range of 3.0-5.0 also appeared to provide a low interfacial tension between the aqueous and oil phases which facilitated the transport of calcium into the aqueous phase. (Kuehne *et al*., 2005)

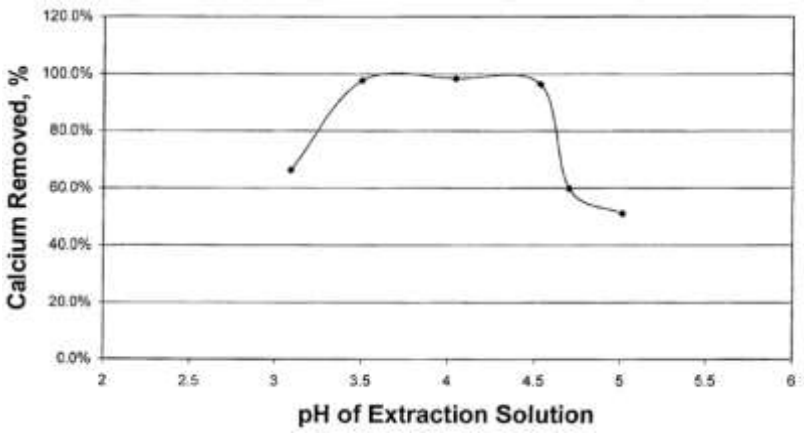

Figure 9. Calcium removal as a function of the pH value of the extraction solution (Kuehne *et al*., 2005).

After mixing the petroleum feedstock with the extraction solution, the mixture was separated into aqueous phase and calcium-reduced oil phase. The phases could be separated by a simple decanting process if no emulsion was formed during the process. However, an emulsion was often formed and needed to be broken or demulsified before the separation. The mixing process was generally done at a temperature below the boiling point of water at the process pressure. Typically, temperatures ranged from 25 to 200 °C and the pressure was greater than the atmospheric pressure. (Kuehne *et al*., 2005)

Adams *et al.* (1965) patented a process for removing metals from high boiling hydrocarbon fractions with hydrofluoric acid. The hydrofluoric acid reacted with the metallic contaminants to form finely divided solid particles. The reaction effluent was treated to remove the acid by, for example, flashing or stripping with steam before the remaining oil and solid metallic particles were separated. The metals were recovered as a solid containing 5-20 wt% of metal in a carbonaceous, coke-like material. This metallic coke-like material was insoluble in both the oil and the aqueous phases while the bulk of the porphyrin molecule remained in the oil phase. The metallic contaminants could be removed by filtration. This demetallization process differed from other methods using acids because the metal contaminants were recovered as solid precipitates rather than as acid-soluble compounds or heavy sludge. (Adams *et al*., 1965)

According to the patent of Adams *et al.*, operating the demetallization process continuously was preferable since no separate layers of acid and hydrocarbons were allowed to form in a continuous process. A process flow chart containing a distillation unit of crude oil and the demetallization process is presented in Figure 10. The distillation unit could be an atmospheric distillation or a combination of atmospheric and vacuum distillation towers. The hydrofluoric acid could be continuously removed as vapor from the flash tower and recycled back to the process. (Adams *et al*., 1965)

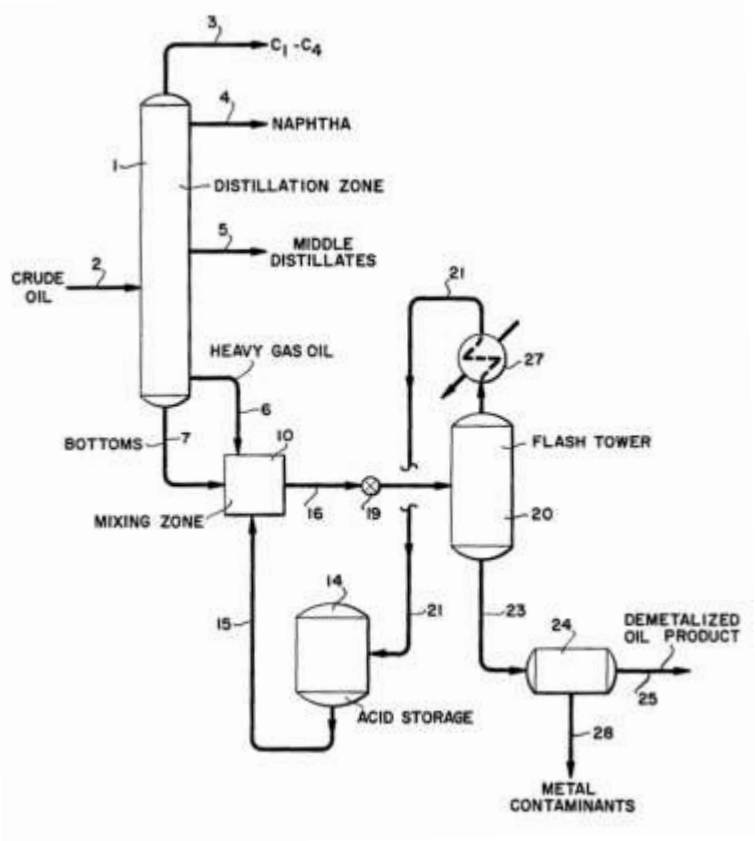

Figure 10. Distillation unit and demetallization process with hydrofluoric acid (Adams *et al*., 1965).

The concentration of aqueous hydrofluoric acid used in the process was from 50 % to nearly 100 %. However, high concentration (70-99 %) was more preferable. The temperature of the demetallization was preferably between 120 and 180 °C and the pressure in the mixer needed to be sufficient to maintain the reactants in liquid phase at the temperature used. The oil and acid could be intensively agitated to obtain a good contact since the formation of emulsions between the oil and the acid was not a problem as the separation was done by flashing. After mixing, the effluent mixture passed through a pressure relief valve to the flash tower where the acid vapors were flashed overhead

and condensed before recycling. The process could recover a hydrocarbon yield of over 99 %. (Adams *et al*., 1965)

4.2.2 Demetallization by phosphorous compounds

Kukes and Battiste (1985) patented a demetallization process which utilized phosphorous acid. Phosphorous acid reacted with the metals to form oil-insoluble compounds that could be removed from the oil stream by any conventional method such as filtration, centrifugation or settling/decantation. Phosphorous acid (H_3PO_3) was a more effective demetallizing agent than phosphoric acid (H_3PO_4) and was found to be particularly effective in vanadium removal. (Kukes & Battiste, 1985)

The phosphorous acid used in the process was an aqueous solution containing about 40-80 wt% of phosphorous acid. A gas could be present during the mixing of the hydrocarbon stream and the phosphorous acid as the gas enabled high-pressure operation to be achieved. Gases such as hydrogen, nitrogen, air, methane and carbon dioxide were suitable for the process. When hydrogen was utilized, the pressure of the demetallization process was preferably 800-7000 kPa. The most preferable temperature range for the process was between 350-450 °C. According to the patent, the demetallization process with phosphorous acid was a suitable pretreatment step before hydrodesulphurization. (Kukes & Battiste, 1985)

A demetallization process in which the hydrocarbon feedstock was contacted with a phosphorous compound to form oil-insoluble compounds was also patented by Kukes (1985). Phosphine, hydrocarbylphosphines, hydrocarbylphosphites, hydrocarbylphosphates, hydrocarbylphosphonates, hydrocarbylphosphine oxides, hydrocarbylthiophosphites and hydrocarbylphosphine sulfides were suitable phosphorous compounds for the process. These compounds reacted with the metals present in the hydrocarbon feed to form oil-insoluble compounds that could be removed from the hydrocarbon feed by conventional method such as filtration, centrifugation or

decantation. This demetallization process was particularly applicable for the removal of vanadium and nickel. (Kukes, 1985)

In the demetallization process of Kukes, mixing hydrogen with the mixture of hydrocarbon feed stream and the phosphorous compound was found to enhance the metal removal. Adding the gas allowed operating the process in high pressure. Compared to gases such as nitrogen, methane and carbon dioxide, the utilization of hydrogen had desirable effects on the process such as reduced coking. (Kukes, 1985)

According to the patent, temperature was preferably between 300-450 °C and the pressure 800-17300 kPa. If the phosphorous compounds were gaseous or liquid, they could be pumped in that form into the hydrocarbon feed. In the case the phosphorous compound was solid, it could be dissolved in the hydrocarbon feed stream or in any suitable solvent. Preferably, the concentration of the phosphorous compound was in the range of about 0.05 to about 5 wt% based on the weight of the hydrocarbon feed stream. If an excess of the phosphorous compound was used, the excess phosphorous compound was removed from the hydrocarbon stream by distillation if the volatility of the phosphorous compound was suitable. If distillation could not be utilized, the excess phosphorous compound could be thermally decomposed which generally converted it to oil-insoluble form which was then removed simultaneously with the metal contaminants. (Kukes, 1985)

Krambeck *et al.* (1987) found that water-soluble phosphorous compounds were capable of forming a compound or a complex with vanadium and nickel present in petroleum. As a result, a significant quantity of the metal could be removed from the oil phase to the aqueous phase. They patented a demetallization process in which the hydrocarbonaceous feedstock was extracted with an aqueous solution of phosphorous compound. The hydrocarbonaceous feedstock was contacted with a relatively substantial quantity of water in which one or more phosphorous compounds were dissolved. The phosphorous compounds formed compounds or complexes with the

vanadium and nickel components present in the oil feed and extracted the metals into the aqueous phase. Examples of suitable and effective phosphorous compounds were P_2O_5, H_3PO_4, $(NH_4)_3PO_4$, $(NH_4)_2HPO_4$, $(NH_4)H_2PO_4$, $(NH_4)H_2P_2O_7$, $H_4P_2O_7$, H_3PO_2 and H_3PO_3. (Krambeck *et al*., 1987)

The hydrocarbon stream could be contacted with the aqueous phosphorous solution by continuous countercurrent extraction. The hydrocarbon stream was fed into the bottom of the extraction tower while the aqueous phosphorous stream was introduced to the top of the tower as shown in Figure 11. In the extraction tower, the phosphorous compounds reacted or formed complexes with the vanadium and nickel present in the oil. As a result, these metals were extracted from the oil phase into the aqueous phase which was withdrawn from the bottom of the extraction tower. The phosphorous-metal compounds/complexes could be separated from the water and therefore, the water could be recycled back to the process. (Krambeck *et al*., 1987)

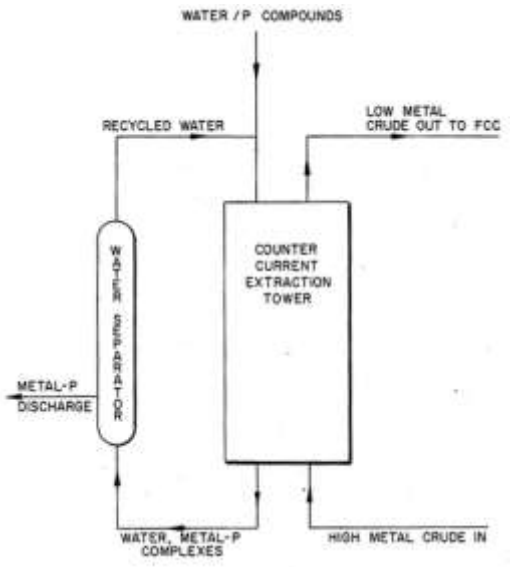

Figure 11. Simplified process flow diagram of the demetallization process by countercurrent extraction (Krambeck *et al*., 1987).

Temperature in the extraction was preferably from about 80 °C to about 200 °C. If the temperature was above 100 °C, pressurized vessels were required to maintain a liquid system. However, if the densities of the aqueous phosphorous solution and the oil were very close and the interfacial tension low, continuous countercurrent extraction was not applicable and some other contacting procedure needed to be utilized. (Krambeck *et al*., 1987)

4.2.3 Demetallization by supercritical water

Utilizing supercritical water (SCW) provides a new approach for the removal of metals from heavy oils. Metal removal is done above the critical point of water in the absence of catalyst and without addition of hydrogen. SCW functions as a solvent and a hydrogen donor. (Mandal *et al*., 2012)

The properties of SCW differ significantly from the properties of water at ambient temperature. The dielectric constant of water is 78.5 at 25 °C. The value drops with increasing temperature and at the critical point of water the dielectric constant is around 6. The relatively low value results from the reduced number of hydrogen bonds. Due to the low dielectric constant, nonpolar organic substances and gases can be dissolved in SCW. (Bröll *et al*., 1999)

The purpose of using SCW is to break the nitrogen-metal bonds of the metal porphyrins. The demetallization occurs at high temperatures and pressures as the critical point of water is at 374 °C and 22.1 MPa. The effect of temperature on reaction of metal porphyrins in SCW is remarkably high while the water partial pressure has a moderate effect. The metal porphyrin conversion increases with reaction time and higher temperature as can be seen in Figure 12. However, the reaction did not complete at the high temperature of 490 °C and the conversion did not change significantly after 90 minutes of reaction time. This indicates the occurrence of a reversible reaction and establishment of the equilibrium after 90 min at 490 °C. In the experiments, the water

partial pressure was 25 MPa and toluene was added as a co-solvent with SCW. Solid metal porphyrins are stable below 400 °C with water partial pressure of 25 MPa in the absence of toluene. (Mandal *et al*., 2014)

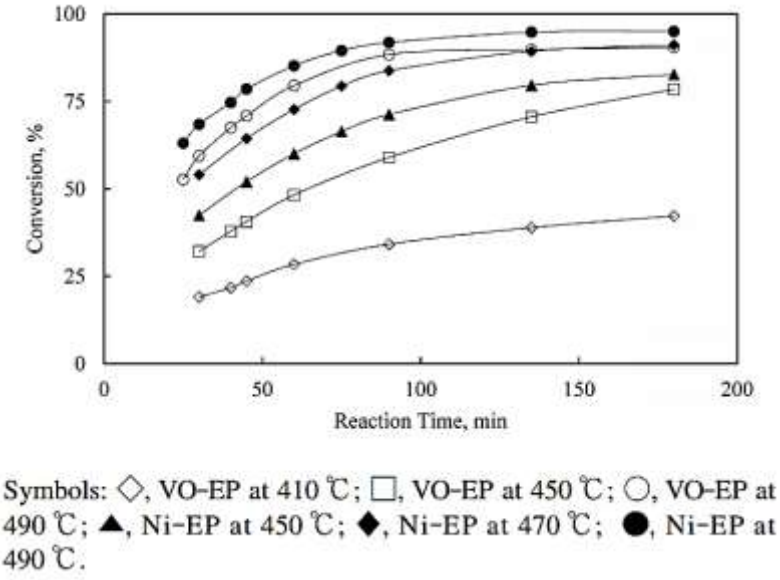

Figure 12. Conversion of vanadyl etioporphyrin (VO-EP) and nickel etioporphyrin (Ni-EP) at different temperatures as a function of reaction time (Mandal *et al*., 2014).

Mandal *et al.* studied the effect of water partial pressure between 25-45 MPa at 450 °C in a toluene environment. The conversion of metal porphyrins was found to increase with higher water partial pressure. The conversion of vanadyl etioporphyrin and nickel etioporphyrin as a function of water partial pressure is shown in Figure 13. (Mandal *et al*., 2014)

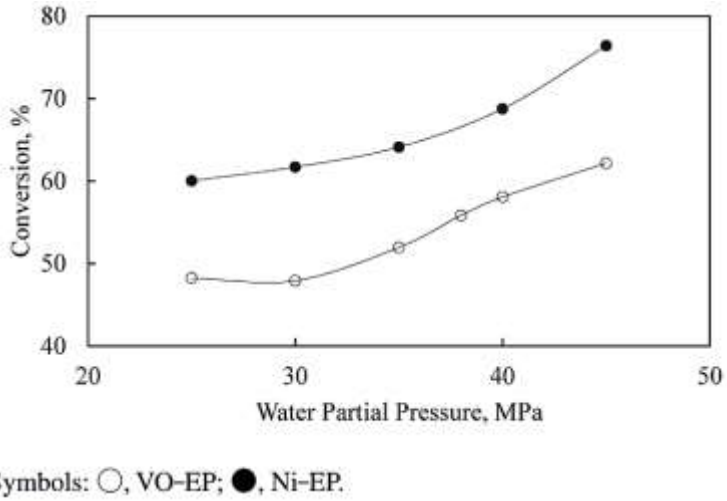

Figure 13. Conversion of vanadyl etioporphyrin and nickel etioporphyrin as a function of water partial pressure (Mandal *et al*., 2014).

Mandal *et al*. used an 8.8 mL batch reactor in their laboratory experiments. The reactor was loaded to an electric furnace which was heated to the planned temperature. The reactor was shaken in a front-back motion and after a specific reaction time it was removed from the furnace and quenched in an ice bath. The water was separated using a separating funnel and the reaction products were collected by washing with xylene. (Mandal *et al*., 2012; Mandal *et al*., 2014)

The central metal group was found to stabilize the porphyrin molecule with respect to hydrogenation and ring fragmentation (Bonné *et al*., 2001). Metal porphyrins are hydrogenated several times successively until the porphyrin macromolecule is disrupted and it loses the porphyrinic character. SCW acts as a hydrogen donor in the hydrogenation reactions. When the covalent metal-nitrogen bonds are weakened, the porphyrin macromolecule may become more vulnerable to hydrogenation reactions and ring fragmentation caused by, for example, thermal cleavages. Metal is removed from the porphyrin structure by reacting with the OH of SCW and by ring fragmentation due

to the instability of metal-free porphyrins under the reaction conditions. (Mandal *et al*., 2014)

The reaction mechanism could be explained using free radical mechanism. The reaction was initiated by producing H, OH and metal porphyrin radicals and propagated by forming radicals of hydrogenated compounds and also metal hydroxide and porphyrin radicals. Termination occurred when free radicals combined to form stable products. The mechanism is shown in the following equations. (Mandal *et al*., 2014)

Initiation:

$$H_2O \rightarrow H\cdot + \cdot OH \quad (5)$$

$$MP \leftrightarrow MP\cdot \quad (6)$$

Propagation:

$$MP\cdot + 2H\cdot \leftrightarrow IHC\cdot \quad (7)$$

$$MP\cdot + \cdot OH \rightarrow M(OH)\cdot + P\cdot \quad (8)$$

Termination:

$$P\cdot \rightarrow \text{Stable ring fragmented product} \quad (9)$$

$$M(OH)\cdot + \cdot OH \rightarrow \text{Inorganic metal} \quad (10)$$

$$IHC\cdot + H\cdot + \cdot OH \rightarrow \text{Inorganic metal + ring fragmented product + } H\cdot \quad (11)$$

$$H\cdot + \cdot OH \rightarrow H_2O \quad (12)$$

Symbols: MP, metal porphyrin; IHC, intermediate hydrogenated compound; M, metal.

However, the fate of the central metal group in the reaction of metal porphyrins under SCW conditions was obscure. The formation of metal hydroxides, metal oxides and metal ion was probable. After removing the metal, the porphyrin structure became very unstable under the experimental conditions and decomposed into light hydrocarbons. (Mandal *et al*., 2014)

Supercritical water can remove metals from metal porphyrins without the addition of a catalyst when the temperature is above 400 °C and the water partial pressure is 25 MPa. The metal removal increased nearly exponentially with the conversion at all temperatures. At the highest conversion level, approximately 80.3 % of vanadium and 76.4 % of nickel were removed. The SCW based demetallization process has the potential to remove metals, such as nickel and vanadium, from the metal porphyrins. However, additional study is required to understand the fate of the metals after the reactions before the process can be made industrially viable. (Mandal *et al*., 2014)

4.2.4 Photochemical denitrogenation and desulphurization

Nowadays, the removal of nitrogen from VGO is carried out via a catalytic hydrodenitrogenation and simultaneous hydrodesulphurization process. However, this process requires rather severe conditions, utilization of hydrogen and active catalysts. An alternative process for removing the nitrogen and sulphur compounds simultaneously under moderate conditions and without the need of hydrogen and a catalyst has attracted interest. (Shiraishi *et al*., 2001)

A photochemical denitrogenation and desulphurization process is based on a combination of UV irradiation and liquid-liquid extraction. Two different solvents have been applied for the process: water and acetonitrile. Using oil/water system, the photodecomposition of the sulphur compounds is achieved in the oil phase. This is followed by the transfer of the resulting decomposition compounds into the water phase. In the oil/acetonitrile system, the sulphur compounds are extracted into the acetonitrile phase and there photodecomposed. It is reported that the photodecomposition of nitrogen compounds proceeds faster than that of the sulphur compounds by sunlight irradiation in water. Therefore, the denitrogenation may be performed simultaneously with the desulphurization. (Shiraishi *et al*., 2000)

Shiraishi *et al.* studied both oil/water and oil/acetonitrile systems. A high-pressure mercury lamp was used for producing photoirradiation. In their experiments, Shirashi et *al.* used model oil containing indole, aniline and carbazole and compared the results with results obtained from three actual light oils. (Shiraishi *et al*., 2000)

In oil/water system, indole and aniline photodecomposed faster than carbazole which decomposition was hindered by the presence of double-ring aromatic hydrocarbons, naphthalenes. The denitrogenation yield decreased linearly with increasing naphthalene concentration. However, the denitrogenation rate was found to accelerate by adding hydrogen peroxide. The rate of all model nitrogen compounds increased with increasing H_2O_2 concentration. Hydrogen peroxide affects in two different ways: producing hydroxyl radicals and acting as a weak oxidizing agent. Direct photodecomposition of H_2O_2 produces hydroxyl radicals which react with the nitrogen compounds. As a weak oxidizing agent, H_2O_2 oxidizes the photoexcited nitrogen compounds, which also accelerates the rate of photodecomposition. The photodecomposed nitrogen compounds were quickly removed from the oil phase into the water where they were found to appear as NO_3^- ions. (Shiraishi *et al*., 2000)

In oil/acetonitrile system, the extraction yield of the nitrogen-containing compounds was greater than that of the sulphur-containing compounds due to the higher polarity of nitrogen. After dissolving in acetonitrile, they were photoirradiated. Similarly as in the oil/water system, the photodecomposed nitrogen compounds were as NO_3^- ions. In oil/acetonitrile system, the presence of naphthalene did not decrease the photoreactivity of nitrogen compounds. (Shiraishi *et al*., 2000)

Shiraishi *et al*. were able to reduce the nitrogen content to less than 20 % of the feed concentration using the oil/water system. However using acetonitrile, the nitrogen content was successfully decreased to less than 3 % of the feed concentration. Both systems enabled simultaneous removal of nitrogen and sulphur. (Shiraishi *et al*., 2000)

After experimenting with light oils, Shiraishi *et al.* studied denitrogenation and desulphurization of VGO using oil/acetonitrile system. Due to its high viscosity at room temperature, VGO was diluted with an n-decane solvent at various volume ratios. The VGO/decane solutions were mixed with acetonitrile and then photoirradiated. The photoirradiation was done under atmospheric pressure and the temperature of the mixture was about 50 °C. The nitrogen concentration in the VGO decreased already when contacted with acetonitrile but it decreased dramatically during photoirradiation. Therefore, the nitrogen compounds efficiently photodecomposed in acetonitrile into highly polarized compounds such as NO_3^- ion. As can be seen in Figure 14, the denitrogenation rate was found to increase when VGO/decane and VGO solution/acetonitrile volume ratios decreased. The data points for zero irradiation time are those obtained by simply mixing the two phases. (Shiraishi *et al*., 2001)

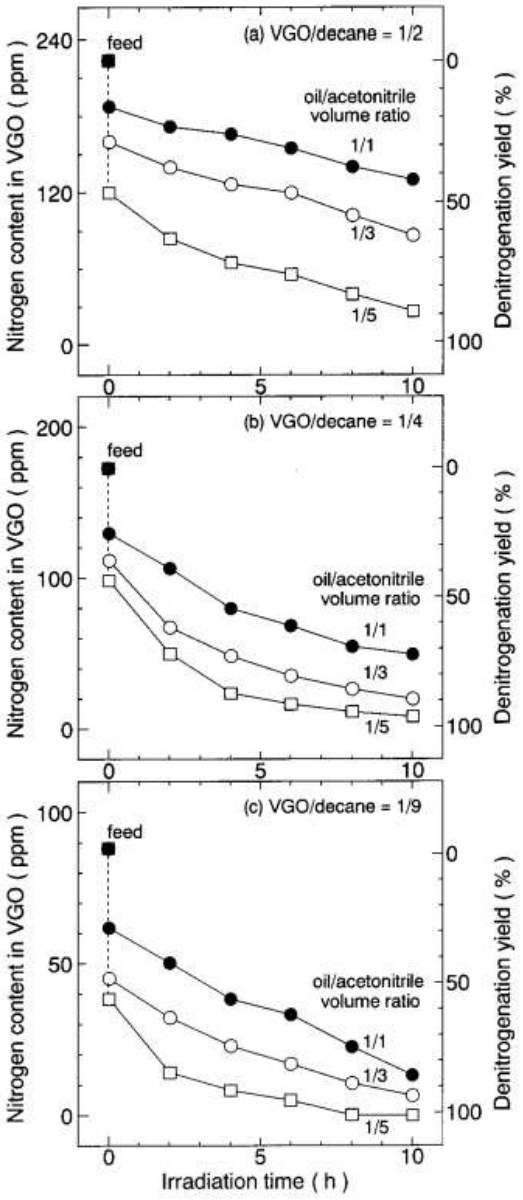

Figure 14. The decrease in the total nitrogen content in VGO during photoirradiation of an oil/acetonitrile system using different VGO/decane and oil/acetonitrile volume ratios (Shiraishi *et al*., 2001).

In the experiments, the photoirradiation time was 10 hours. The nitrogen content of VGO was decreased to less than 1 % of the feed concentration when the oil/acetonitrile and VGO/decane volume ratios were 1/5 and 1/9, respectively. Similarly, the

desulphurization rate was found to increase when VGO/decane and oil/acetonitrile volume ratios decreased. As a result, also the sulphur content was decreased to less than 1 % of the feed concentration. (Shiraishi *et al*., 2001)

5 Advantages and disadvantages of the methods

In this chapter, the advantages and disadvantages of the impurity removal methods presented in chapter 4 are discussed and the methods are compared to each other. One process is chosen for prestudy which is carried out in the applied part of this thesis. The reasoning behind the selection is presented.

5.1 Comparison of the methods

The temperatures, pressures, solvents and reagents used in the SDA, demetallization processes by acids, phosphorous compounds and SCW as well as in photochemical denitrogenation are summarized in Table 2. The photochemical denitrogenation has the mildest operating conditions while the process utilizing SCW requires the most extreme conditions. Due to the high temperature and pressure in the SCW process, the hydrocarbons may start to decompose during the process.

Table 2. Temperatures, pressures, solvents and reagents used in each impurity removal process.

Impurity removal process	Temperature (°C)	Pressure (kPa)	Solvent/reagent
SDA	80–250	2000–4000	light paraffinic solvent (C_3-C_7)
Demetallization by acids	25–200	101–2000	H_2SO_4, CH_3COOH + alkaline material, HF
Demetallization by phosphorous compounds	100–450	101–17500	various suitable phosphorous compounds including phosphorous acid, in certain processes also hydrogen or water
Demetallization by SCW	> 400	> 25000	water + toluene
Photochemical denitrogenation	50	101	n-decane + water or acetonitrile

The National Fire Protection Association (NFPA) has developed a system for identifying hazards associated with materials. The system provides basic information for emergency personnel responding to a fire or spill and for those planning the emergency response. It indicates the health hazard, flammability, reactivity and special hazards for many common chemicals. The hazards are rated from 0 to 4 where 0 indicates the least hazardous and 4 the most hazardous. (NFPA, 2012) The reactivity of a chemical describes the reactivity with water and the capability of detonation or of explosive reactions. The special hazards indicate if a chemical functions as an oxidizing agent (OX) or if it shows unusual reactivity with water (~~W~~). (Northeastern University, 2015) The hazard ratings available for the chemicals used in the impurity removal processes are presented in Table 3.

Table 3. NFPA ratings available to chemicals used in the impurity removal processes (Northeastern University, 2015).

		NFPA hazard rating system			
Impurity removal process	**Chemical**	**Health**	**Flammability**	**Reactivity**	**Special information**
SDA	Propane	1	4	0	
	Butane	1	4	0	
	Pentane	1	4	0	
	Hexane	1	3	0	
	Heptane	1	3	0	
Demetallization by acids	H_2SO_4	3	0	2	~~W~~
	CH_3COOH (glacial)	2	2	2	
	NaOH	3	0	1	
	KOH	3	0	1	
	HF	4	0	0	
Demetallization by phosphorous compounds	Phosphine	3	4	1	
	H_3PO_4	2	0	0	
	Hydrogen	0	4	0	
Demetallization by SCW	Toluene	2	3	0	
Photochemical denitrogenation	Decane	0	2	0	
	Acetonitrile	2	3	0	

~~W~~: reacts strongly with water

The NFPA hazard rating system gives valuable information about the chemicals and their properties. By utilizing chemicals with low ratings, the hazards of a process can be reduced. Unless a certain chemical is critical for the process, replacing it with a less hazardous alternative is preferable.

Hydrofluoric acid has the most hazardous rating (4) for the health. It is caustic to respiratory tract and toxic if inhaled. It causes severe skin burns and eye damage and may cause frostbite. (Airgas, 2015) Moreover as presented in chapter 4.2.1, the hydrofluoric acid preferred in the demetallization process has a really high concentration (70-99 %). Therefore, preferring the use of other chemicals could reduce the health risks.

As can be seen in Table 3, light paraffinic hydrocarbons, hydrogen and phosphine are extremely flammable. They pose a threat of causing an explosion. Therefore, their utilization and handling requires special caution in order to safely operate the process. If the risk of explosion cannot be minimized to an acceptable level and the chemicals handled safely, the process is not implementable.

The properties of chemicals affect the material choices as the chemicals can cause corrosion. The main parameters affecting the acid corrosion are temperature, acid concentration, the hydrodynamic flow rate and the presence of oxidizing agents. Formation of, for example, metal sulfate or fluoride layer protects the alloys but if the layer is torn, serious corrosion will occur. The presence of oxidizing agents increases the corrosion rate. (Ropital, 2009) For example for the handling of sulphuric acid, austenitic stainless steels have a good resistance only up to 65 °C over the entire concentration range. Some nickel-molybdenum alloys can be used even in temperatures above 120 °C. However, these alloys suffer serious corrosion in the presence of oxidizing agents and in aqueous acid systems. The corrosion rates of nickel-base alloys generally increase with acid concentration up to 90 % but higher concentrations are usually less corrosive. (Davis, 2000) Compromises between the operating conditions and acid concentration might need to be done in order to find suitable materials.

The materials used in SCW applications must simultaneously be resistant to high temperatures and pressures and also to corrosion by substances employed (Bröll *et al*., 1999). The most commonly used reactor materials are stainless steels and nickel-base alloys. The alloying elements have to form an oxide layer which completely covers the alloy. Chromium as an alloying element improves the resistance against acidic and oxidizing media while nickel improves the corrosion resistance in alkaline environments. However, chromium loses its protective effect with increasing temperature due to chromate formation. Chromate formation typically occurs when temperature is above 200-250 °C resulting in high corrosion rate. Anions can also destroy the oxide film or act

as oxidizing agents corroding the metals. More basic physical and chemical data is required and extensive long-time studies need to be performed to gain more information about the corrosion resistance of materials in SCW. (Kritzer, 2004)

The demetallization process by SCW and the photochemical denitrogenation are novel processes. Therefore, they are not as technically mature as SDA and demetallization by acids and phosphorous compounds. The lack of technical maturity is a disadvantage of these processes as they require more research and development before they can be operated in an industrial scale. Moreover, as finding suitable materials for SCW is problematic, the demetallization process utilizing SCW is currently not feasible. However, utilizing water as the reagent is an interesting option and subject of research as it could eliminate the need of using toxic and flammable chemicals.

Equipment required for the impurity removal in the more technically mature processes is presented in Table 4. Depending on formation of an emulsion, the demetallization processes by acids may require a unit for breaking or demulsifying the emulsion. Generally, the more equipment is required in a process, the more expensive the investment is. Moreover, the amount of process equipment affects the maintenance costs and the required land area. As the new impurity removal process would be a part of an existing refinery production line, the area available for construction is limited. If the area close to the existing production line is too small, the new process could be constructed slightly further increasing the pipeline and pumping costs.

Table 4. Equipment required in different impurity removal processes.

Impurity removal process	Equipment for removing impurities
SDA	Extraction tower, 2 flash towers, 2 strippers
Demetallization by acids	Mixer, decanter
	Mixer, flash tower or stripper, filter
Demetallization by phosphorous compounds	Mixer, decanter or filter, possibly a distillation tower for the removal of excess phosphorous compounds
	Extraction tower, water separator

An advantage of SDA is the possibility to recycle the solvent. Because SDA is a physical method, the impurity removal is not based on chemical reactions and the separation of solvent is straightforward using flash towers and strippers. In the experiments of photochemical denitrogenation and desulphurization, the removal of nitrogen and sulphur was found to increase when the amount of solvent increased. High impurity removal rate was achieved using significant quantities of solvent compared to the amount of oil treated. Consequently, recycling the substantial amount of solvent could be challenging and cost-inefficient. If the solvent cannot be reused, the process would require an excessive fresh solvent stream which would not be feasible.

Furthermore, the photochemical denitrogenation and desulphurization process is designed for the removal of nitrogen and sulphur impurities while the other methods presented in chapter 4 are for the demetallization of VGO. SDA removes simultaneously the asphaltenes and metals. As the objective of the photochemical denitrogenation and desulphurization differs from that of the other methods, the photochemical process cannot be directly compared to the demetallization processes. Depending on the impurity levels of VGO, denitrogenation would be more interesting if the metal concentration in the feedstock was low but the nitrogen and sulphur content high.

5.2 Selection of one process for prestudy

The most interesting methods for the impurity removal of VGO are SDA and demetallization using phosphorous compounds. The possibilities of SDA have already been noticed in Neste and the process has been studied for years. Currently, a SDA process unit is under construction in Porvoo refinery. However, the SDA will be used for heavier feedstock than VGO to reduce the asphaltene content in the feed. The process can reduce the asphaltene and metal concentrations but not completely remove those impurities. VGO may be too light to achieve a significant and cost-effective reduction in the impurity levels.

The patents made of the demetallization processes with phosphorous compounds were published in the 1980s and thus, they have already expired. In addition, no licenses for the demetallization process were found. Therefore, the process could be freely designed. Compared to SDA, the applicability of this demetallization method has not yet been studied and choosing this for the prestudy would provide new information.

A valuable outcome of this thesis is providing new information about the impurity removal systems. Therefore, the demetallization process by phosphorous compounds was chosen for prestudy. The demetallization process will be applied as a pretreatment process before hydrodesulphurization of VGO in order to reduce the deactivation of hydrotreatment catalyst. The prestudy is carried out in the applied part of the thesis.

APPLIED PART

6 Designing of an impurity removal unit

The amount of VGO fed to the HDS process is 300 tons/h and it contains 10 ppm of metal impurities. VGO with 10 ppm of metal impurities is applied in this work as an example of a low-quality VGO. The aim is to reduce the amount of metal impurities by applying a pretreatment process which utilizes phosphoric acid. The demetallization process extends the HDS catalyst lifetime and therefore, the catalyst can be changed less frequently.

The phosphorous compound used in the demetallization process must be safe to operate and available in bulk quantities. Therefore, phosphoric acid was chosen as the demetallizing agent over phosphorous acid. Phosphorous acid is an unstable substance which converts to phosphoric acid and phosphine when heated. The decomposition of phosphorous acid is presented in Equation 13. (Pauling, 1970) The formed phosphine (PH_3) is extremely flammable. Its autoignition temperature is 38-100 °C depending on the concentration and diluent. (Pohanish, 2012) Due to the formation of phosphine, the utilization of phosphoric acid in the demetallization process is preferred over phosphorous acid.

$$4\mathrm{H_3PO_3} \rightarrow 3\mathrm{H_3PO_4} + \mathrm{PH_3} \tag{13}$$

The amount of experimental data about the metal impurity removal capacity of H_3PO_4 is limited. The data found is presented in Table 5. As can be seen, the impurities studied are often limited to only nickel and vanadium. The metal removal capacities of Eidem (1988) also include the removal of iron and therefore, in this applied part of the thesis the metal impurities, the concentrations of which are reduced by H_3PO_4, are nickel,

vanadium and iron. The concentrations of the other metal impurities present in VGO are not supposed to be affected by H_3PO_4 as no data could be found about their removal rate. To obtain more accurate data for the demetallization of VGO, laboratory experiments should be performed. The amount of H_3PO_4, operating temperature and the initial concentration of impurities affect the removal capacity of H_3PO_4 and therefore, laboratory experiments would provide valuable information for the process design.

Table 5. Experimental data of the metal removal capacity of H_3PO_4.

			Removal of impurities (weight-%)			
Acid	**T (°C)**	**Weight-% of acid in the mixture**	**V**	**Ni**	**Fe**	**Source**
H_3PO_4, 17%	95	29	35	37	NA	(Krambeck *et al*., 1987)
H_3PO_4, concentrated	250	5	18	10	NA	(Abbas *et al*., 2010)
H_3PO_4, 85.1%	260	1	23.4	32.1	21.7	(Eidem, 1988)
H_3PO_4, 85%	400	1.2	60.0	4.1	NA	(Kukes & Battiste, 1985)
H_3PO_4, 85%	400	3.8	41.5	23.5	NA	(Kukes & Battiste, 1985)

NA (not available)

The concentrations of metal impurities in the VGO feed are listed in Table 6. The concentrations are determined based on average concentrations of actual VGO feeds used in the refinery. However, the values are roughly rounded and therefore, do not directly represent the concentration of any actual VGO feed. The metal removal capacities of Eidem (1988) are used in the calculations as the experiments include the removal of iron and the removal percentages are not the highest or the lowest compared to the other publications. Therefore, the calculations would not give either too optimistic

or too poor results but an average removal of the metal impurities. Based on the data, the removal percentages of vanadium, nickel and iron used in the calculations are 23 w-%, 32 w-% and 22 w-%, respectively. To determine the removal percentages more accurately for this demetallization process, laboratory experiments are necessary. The mass flow rates of the metal impurities in the feed and in the demetallized VGO are also presented in Table 6.

Table 6. Concentrations and mass flow rates of metal impurities in the VGO feed and mass flow rates after the demetallization process.

Impurity	Concentration in VGO feed (ppm)	Mass flow rate in the feed (kg/h)	Mass flow rate in VGO after demetallization (kg/h)
Ni	3	0.90	0.61
V	3	0.90	0.69
Na	2	0.60	0.60
Fe	1	0.30	0.23
Ca	0.9	0.27	0.27
As	0.1	0.03	0.03
Total	10	3.00	2.44

The applied part of the thesis is divided into case 1 and case 2. In case 1 operating the HDS process without an impurity removal unit is studied and the HDS catalyst lifetime is calculated. In case 2 the demetallization process is integrated into the HDS process. The demetallization process is designed, the equipment sizing is performed and the costs of implementing this new impurity removal treatment are estimated. Finally, the profitability of the demetallization process is assessed.

7 Case 1. HDS process without a new impurity removal system

In this chapter, the HDS process without the demetallization pretreatment is discussed. The HDS catalyst lifetime is calculated in order to determine how fast the VGO feed with 10 ppm of metal impurities deactivate the catalyst.

7.1 Process description

HDS is the primary sulphur removal technology used in refineries. It is a catalytic process in which the sulphur content in fuels is reduced by reaction with hydrogen at 330-370 °C. (Shekhawat *et al*., 2011) As a result of the reaction, H_2S is formed. Molybdenum is often used to formulate HDS catalysts but tungsten is also effective. These metals are used in combination with nickel or cobalt which acts as a promoter. (Schobert, 2013)

Hydrogen sulphide produced during the HDS must be treated and therefore, the H_2S/H_2 stream is fed to an amine scrubber to absorb the H_2S. After the amine scrubbing, H_2S is desorbed and sent to a sulphur recovery process. (Shekhawat *et al*., 2011) However, in this thesis the focus is in the beginning of the HDS process and in the reactors. Therefore, the processing of reactor effluent is excluded from this work.

Process flow chart of the examined part of HDS process is presented in Figure 15. The feed is pumped from a storage tank (FA-101) through two heat exchangers (EA-101 and EA-102). In the heat exchangers, the effluent of the last reactor (DC-103) is utilized to heat the feed stream. To raise the temperature even higher, the feed flows to a furnace (BA-101). Then, the hydrodesulphurization occurs in three consecutive reactors (DC-101…103). Hydrogen is added to the feed before the furnace and in the first reactor.

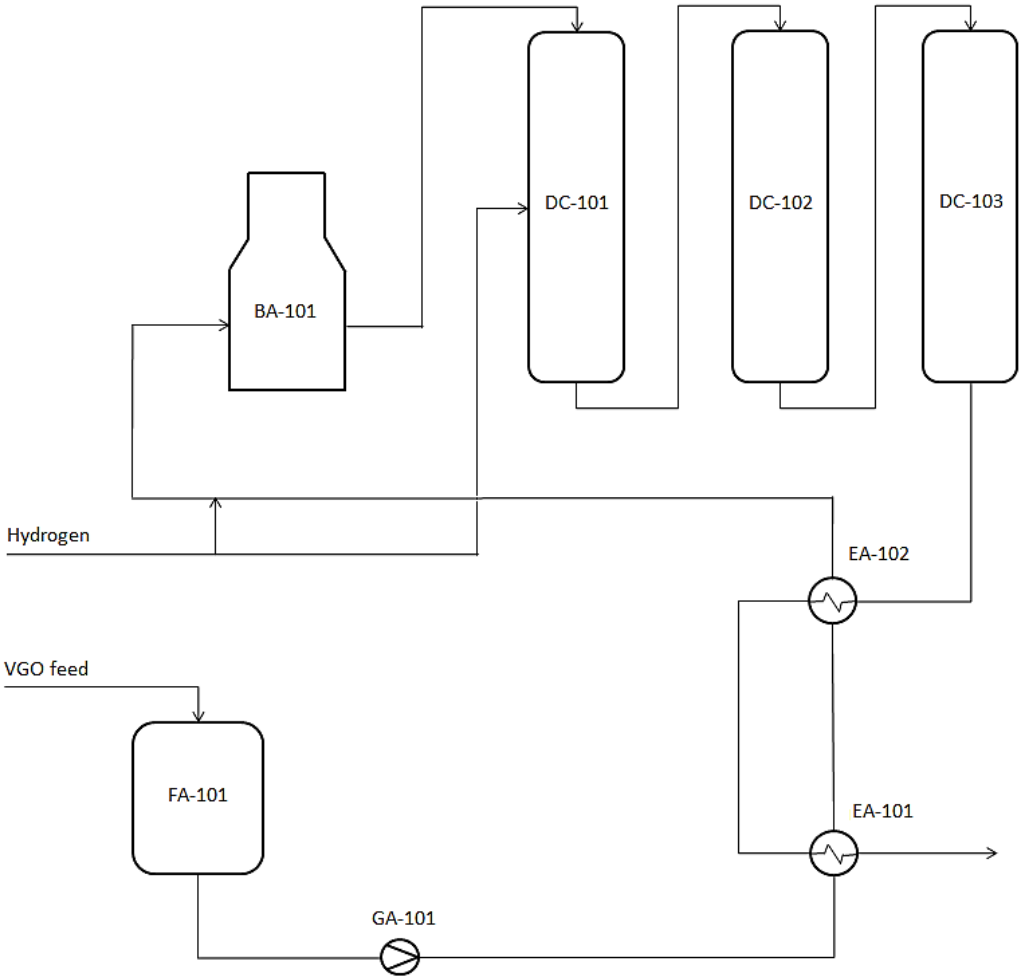

Figure 15. Process flow chart of the examined part of HDS process.

7.2 Catalyst lifetime

The HDS catalyst is considered to be deactivated when it has 30 % left of the initial activity. Guard bed is utilized to adsorb the metal impurities and to limit the deactivation of HDS catalyst. Based on the experience in Neste, the guard bed is estimated to adsorb 25 w% of the metal impurities in the feed until its adsorption capacity is full. The total adsorption capacity is around 10 % of the mass of guard bed. As the mass of guard bed catalyst used in the process is around 12 tons, the adsorption capacity of the guard bed

is 1.2 tons of metal impurities. The amount of different metal impurities adsorbed by the guard bed is presented in Table 7. The process is started in week 1 and it can be seen that the adsorption capacity is full during week 10. As a result, the guard bed cannot adsorb more and would let all the metal impurities go through to the HDS catalyst after week 10.

Table 7. Accumulation of metal impurities in guard bed.

			Accumulation of impurities in the guard bed (kg)						
Week	**Feed stream (t/h)**	**Feed stream (t/wk)**	**As**	**Ca**	**Fe**	**Na**	**V**	**Ni**	**Total**
1	300	50400	1.3	11.3	12.6	25.2	37.8	37.8	126
2	300	50400	2.5	22.7	25.2	50.4	75.6	75.6	252
3	300	50400	3.8	34.0	37.8	75.6	113.4	113.4	378
4	300	50400	5.0	45.4	50.4	100.8	151.2	151.2	504
5	300	50400	6.3	56.7	63.0	126.0	189.0	189.0	630
6	300	50400	7.6	68.0	75.6	151.2	226.8	226.8	756
7	300	50400	8.8	79.4	88.2	176.4	264.6	264.6	882
8	300	50400	10.1	90.7	100.8	201.6	302.4	302.4	1008
9	300	50400	11.3	102.1	113.4	226.8	340.2	340.2	1134
10	300	50400	12.6	113.4	126.0	252.0	378.0	378.0	1260

The deactivation of the HDS catalyst is calculated using research data of Neste. Based on the data, the activation of the HDS catalyst will go below 30 % of the initial activity during week 9. Therefore, the HDS catalyst lifetime is 8 weeks when VGO feed with 10 ppm of metal impurities is used. The HDS catalyst is deactivated before the adsorption capacity of the guard bed is full. Due to the short catalyst lifetime, the process is shut down after every 8 operating weeks resulting in lost profit. Both the HDS and the guard bed catalyst are changed during the shutdowns. As the shutdowns are required often, the process is under normal operating conditions only for short periods of time. Therefore, the process risks are higher as the most of process deviations occur when the process is being shut down or started after maintenance.

By reducing the metal impurity level before the HDS, the catalyst lifetime could be extended and the shutdowns would occur less frequently. The costs of changing the HDS catalyst and the guard bed during one shutdown are equal in cases 1 and 2. The costs of changing the catalysts are discussed in chapter 8.3.2.

8 Case 2. Impurity removal integrated in the HDS process

In this chapter, the demetallization process by phosphoric acid is designed and the sizing of required equipment is performed. The profitability of the process is evaluated and in the end of this chapter, the focus is on safety issues.

8.1 Process design

The demetallization with phosphorous compounds can be realized using two different approaches. The first process option is countercurrent extraction which was described in the patent of Krambeck *et al.* (1987). The other option is to use a mixer followed by a decanter or filter (Kukes, 1985).

The extraction requires significant amount of water. According to Krambeck *et al.* (1987), the weight ratio of water to oil was most preferably 0.2-1 meaning 60-300 t/h of water in the demetallization process. Therefore, the capacity of handling, cleaning and recycling the water should be enormous. Due to the large amount of water required in the extraction, using a mixer was preferred as the process option.

8.1.1 Process flow chart

The mixing is done in a static mixer, a tubular device which consists of stationary mixing elements. The mixing elements split the fluid flow into several partial flows which are then recombined to form a mixture. Both the degree of homogeneity and the pressure

drop increase with the number of mixing elements. Because of no moving parts, they require little or no maintenance. Another advantages are short residence times and that there are no power requirements other than pumping the fluid. (Coker, 2001) After the mixer, the oil and aqueous phases are separated. For the separation, both a decanter and an electrostatic coalescer are studied but only the decanter is designed.

The demetallization process was chosen to be located between the two heat exchangers (EA-101 and EA-102) of HDS process. Process flow chart of the HDS with the integrated demetallization is presented in Figure 16. VGO feed flows through the heat exchanger EA-101 before it enters the static mixer (GD-101) where phosphoric acid is added to the VGO stream. The operating temperature is around 225 °C and the pressure 60 bar in the mixer. Then, the mixture flows to either a decanter or an electrostatic coalescer (HB-101) where the oil phase is removed from the aqueous phase and fed to the furnace (BA-101) through the heat exchanger EA-102. Finally, the demetallized VGO enters the HDS reactors (DC-101…103).

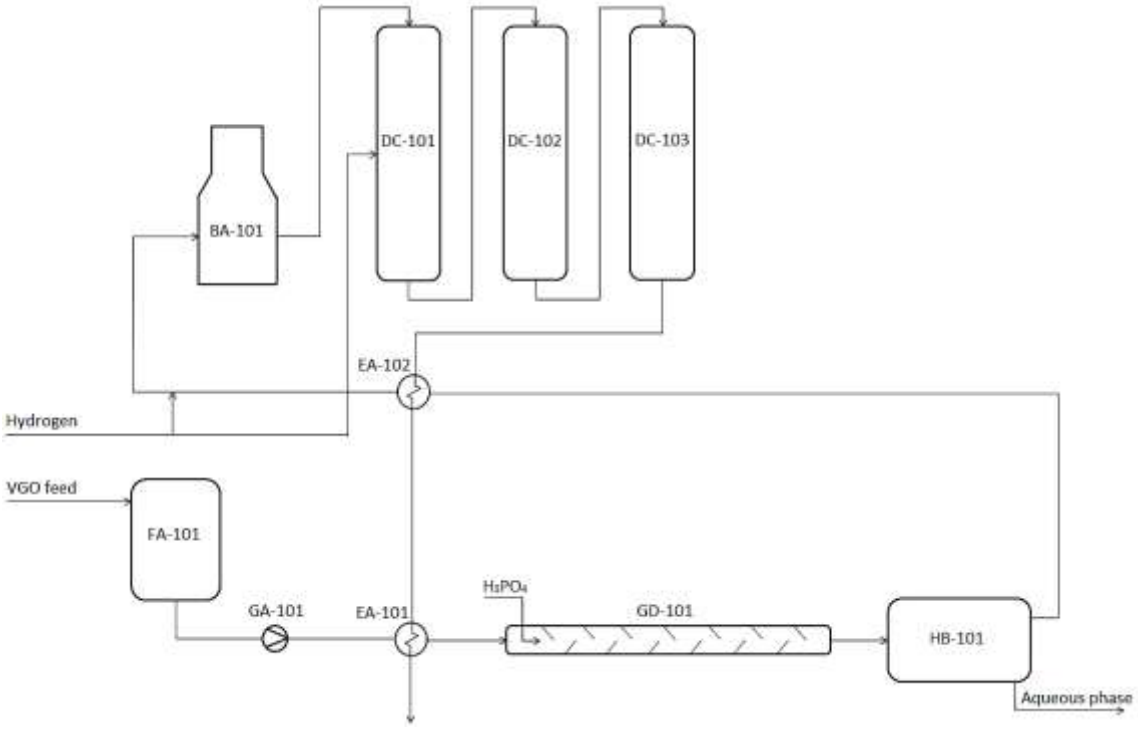

Figure 16. Process flow chart of demetallization process integrated in HDS process.

Even though the demetallization process reduces the amount of metal impurities entering the reactors, the same guard bed will be used in this process as in case 1. The guard bed further extends the HDS catalyst lifetime.

8.1.2 Mass flow rate of phosphoric acid

The amount of H_3PO_4 required in the mixer is calculated based on reactions of the metal impurities with phosphate ions. In petroleum nickel occurs in the +2 valence state while most vanadium atoms have a valence of +4, almost exclusively as vanadium ions VO^{2+} (Mandal *et al*., 2014). Similarly to nickel and vanadium, iron is present in the structures of porphyrin compounds (Leprince, 2001). The reactions with phosphate ions are presented in Equations 14-16.

$$3Ni^{2+} + 2PO_4^{3-} \leftrightarrow (Ni)_3(PO_4)_2 \quad (14)$$

$$3VO^{2+} + 2PO_4^{3-} \leftrightarrow (VO)_3(PO_4)_2 \quad (15)$$

$$3Fe^{2+} + 2PO_4^{3-} \leftrightarrow (Fe)_3(PO_4)_2 \quad (16)$$

Based on the equations, the required molar amount of phosphoric acid is

$$n(H_3PO_4) = \frac{2}{3}n(Ni) + \frac{2}{3}n(V) + \frac{2}{3}n(Fe) \quad (17)$$

The molar flow rates of nickel, vanadium and iron in the VGO feed are presented in Table 8. Utilizing large excess of H_3PO_4 would require more separation capacity for the decanter as the unreacted H_3PO_4 should be removed. However, a small excess of phosphoric compound is necessary in order to remove all the possible metal impurities in a reasonable time. Therefore, the preliminarily estimated amount of H_3PO_4 used in the process is twice the stoichiometric molar amount.

Table 8. Mass flow, molar mass and molar flow of nickel, vanadium and iron in the VGO feed.

Impurity	Concentration (ppm)	m (kg/h)	M (g/mol)*	n (mol/h)
Ni	3	0.9	58.693	15.33
V	3	0.9	50.942	17.67
Fe	1	0.3	55.845	5.37

*Source: (Yaws, 2011)

Based on Equation 17, the stoichiometric molar flow of H_3PO_4 is 25.6 mol/h. Therefore, the molar amount applied in the process is 51.2 mol/h. Based on the molar masses published by Yaws (2011), the molar mass of H_3PO_4 is 97.996 g/mol and therefore, the mass flow of 100 % H_3PO_4 is 5.0 kg/h. However, H_3PO_4 is corrosive and the use of 100 %

H_3PO_4 is not required in the demetallization process. Therefore, an aqueous solution containing 75 w% H_3PO_4 is chosen to be utilized in the process. The mass flow of 75 w% H_3PO_4 is 6.7 kg/h which is rounded to 7 kg/h. The mass flow of H_3PO_4 is rounded to 7 kg/h as the mass flow of VGO is also expressed with one significant number within the accuracy of the thesis.

8.1.3 Physical properties of VGO and phosphoric acid

Physical properties of VGO used in the calculations are listed in Table 9. The density and viscosity of VGO are at 150 °C due to no values in higher temperature were available. The density of VGO at 150 °C is estimated by multiplying the specific gravity of VGO at 150 °C and the density of water at 150 °C. The use of physical properties in a lower temperature than the operating temperature will cause some inaccuracy in the calculations.

Table 9. Physical properties of VGO.

Physical property	**Unit**	**VGO**
Specific gravity (150 °C)	-	0.825*
Density (150 °C), ρ	kg/m^3	760
Kinematic viscosity (150 °C), μ_{kin}	m^2/s	$2.60 \cdot 10^{-6}$**
Dynamic viscosity (150 °C), μ_{dyn}	Pa·s	$2.32 \cdot 10^{-3}$

Source: *(Manning & Thompson, 1995), **(Jechura, 2015)

The density of 75 w% H_3PO_4 at 225 °C is calculated using Equation 18. The densities of liquid pure water and H_3PO_4 at 225 °C were taken from Aspen Plus simulation program and are 836 kg/m^3 and 1700 kg/m^3, respectively.

$$\rho_{H_3PO_4,75\%} = \frac{m_{H_3PO_4} + m_{H_2O}}{\frac{m_{H_3PO_4}}{\rho_{H_3PO_4}} + \frac{m_{H_2O}}{\rho_{H_2O}}} \quad (18)$$

Therefore, the density of liquid, pressurized 75 w% H_3PO_4 at 225 °C is

$$\rho_{H_3PO_4,75w\%} = 1351.5 \frac{kg}{m^3} \approx 1350 \frac{kg}{m^3}$$

8.2 Equipment

The demetallization process consists of the static mixer and either of the decanter or the electrostatic coalescer. In addition, H_3PO_4 is stored in a storage tank before pumping it into the mixer. In this chapter, the preliminary design and sizing of the static mixer and decanter are conducted. The electrostatic coalescer and the storage tank of H_3PO_4 are discussed briefly in the end of this chapter.

8.2.1 Static mixer

In the static mixer, H_3PO_4 reacts with the metal impurities to form water soluble compounds like metal phosphates. As the amount of H_3PO_4 is negligible compared to the amount of VGO, the sizing of the static mixer is calculated using the values of VGO.

A Kenics mixer was chosen to be used as the static mixer in the demetallization process. Kenics mixers are among the most commonly applied static mixers. Designed and manufactured by Chemineer, the Kenics mixers consist of a variety of different mixer designs. The pressure drop through the static mixer depends on the design and whether the flow is laminar or turbulent. Moreover, the type of flow affects the design since some mixers are especially designed for the laminar flow and some for turbulent. (Coker, 2007)

An injection mixer is a suitable design when one flow is much lower than the other (Towler & Sinnott, 2013). As the flow rate of H_3PO_4 is significantly lower than the flow rate of VGO, the streams are mixed using injection in the demetallization process. A design of static injection mixer is can be seen in Figure 17.

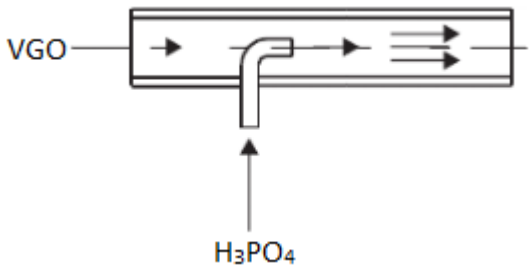

Figure 17. Static injection mixer. Adapted from Towler & Sinnott (2013).

Dimensions of the mixer

The diameter of the static mixer is determined by calculating the economic pipe diameter. The capital cost of a pipe increases with diameter, whereas the pumping costs decrease with increasing diameter. A rule of thumb for the economic pipe diameter that is used in oil refining is presented below (Equation 19). (Towler & Sinnott, 2013) In order to obtain meters from the equation, the units inside the square brackets reduce the extra units.

$$D_{i,optimum} = 3.2\left(\frac{m}{\rho}\right)^{0.5}\left[\left(\frac{1\ s}{1\ m}\right)^{0.5}\right] \quad (19)$$

where D_i = pipe inside diameter, m

m = mass flow rate, kg/s

ρ = density of fluid, kg/m^3

Therefore,

$$D_{i,optimum} = 1.06 \text{ m} \approx 1 \text{ m}$$

The diameter of static mixer is rounded to 1 m. Reynolds number is calculated using Equation 20 to determine whether the flow is laminar or turbulent (Menon, 2015).

$$Re = \frac{\rho D u}{\mu} \tag{20}$$

where Re = Reynolds number

ρ = density of fluid, kg/m^3

D = equivalent diameter, m

u = fluid velocity, m/s

μ = dynamic viscosity of fluid, Pa·s

The fluid velocity *u* is calculated by dividing volumetric flow rate with the cross-sectional area of the pipe. Therefore,

$$Re = \frac{Dm}{\mu\pi\left(\frac{D}{2}\right)^2} = 45714$$

Below a Reynolds number of 2000, the flow in pipes will be laminar. The flow will be critical when the Reynolds number is between 2000-4000 and turbulent above 4000. Therefore, the fluid flow in the static mixer is turbulent. (Menon, 2015)

For the mixing of turbulent flow, a suitable option is to use a mixer which generates controlled vortex structures. The mixing element geometry takes advantage of the naturally occurring vortices induced by the element edges. A vortex generating Kenics mixer called the HEV mixer is presented in Figure 18. (Coker, 2007)

Figure 18. Structure of HEV static mixer (Coker, 2007).

Although for the standard HEV mixer L/D ratio is 1, the L/D for the placing of the HEV into the piping system is nominally 4 due to the vortexes which provide mixing downstream of the mixer. Kenics has specified that three pipe diameters of straight pipe need to be attached to the exit of the mixer. (Couper *et al.*, 2012) To estimate the length of the mixer, the amount of mixing elements need to be determined.

According to guidelines for sizing an Admixer^{TM} for liquid/liquid mixing, the number of elements depends on the Reynolds number and the ratio of fluid viscosities and volumes. In the demetallization process based on the guidelines the static mixer requires four mixing elements because the Reynolds number is above 5000 and the volumetric ratio between VGO and H_3PO_4 exceeds 100:1. (Admix, 1998) To assure the fluids are completely mixed one additional mixing element is added in the preliminary design and therefore, the total of five elements are utilized in the mixer. As the diameter of the mixer is 1 m, the length of the mixing section is 20 m.

However, to provide sufficient reaction time the mixing section is followed by an empty pipe without mixing elements. The liquid hourly space velocity (LHSV) is the reactant liquid flow rate divided by reactor volume and is determined to be 3 h^{-1} in this demetallization process. The length of the static mixer is calculated based on the LHSV and the dimensions of the mixer are summarized in Table 10.

Table 10. Dimensions of the static mixer.

Equipment	Volume (m^3)	Cross-sectional area (m^2)	Inside diameter (m)	Mixing section length (m)	Total length (m)
Static mixer	132	0.785	1.0	20	168

The total length of the mixer is 168 m including the mixing section of 20 m. The mixer requires a large space and therefore, it would need to be constructed further from the HDS process as the space available close to the existing HDS process is limited. Due to the great length, the mixer would rather have bends than be constructed of a straight pipe. In the preliminary design, the mixer is constructed using straight pipes of 10 m which are connected by 180° standard radius elbows to form a compact mixer design. The ratio of elbow radius to pipe diameter is 1 for the standard radius elbow resulting in 1 m elbow radius and approximately 3 m elbow length. Therefore, the mixer consists of 13 straight pipes of 10 m length and 12 standard radius elbows of 180°. The amount and type of elbows affect the pressure drop in the mixer which is discussed next in this chapter.

Pressure drop

As the pressure drop is dependent on the design of the mixer, special data is required from the manufacturer. Therefore, the pressure drop should be determined with the assistance of the manufacturer. The pressure drop in the Kenics mixer can be determined

by multiplying the pressure drop in an empty pipe with a specific coefficient *K*. The equation for calculating *K* in a turbulent flow is presented in Equation 21 and it must be calculated using the data of the manufacturer. (Coker, 2007)

$$K = K_{OT}B \tag{21}$$

where K_{OT} = factor related to the diameter and wall thickness of the mixer

B = factor related to Reynolds number

Some data for calculating the coefficient *K* has been published. Values for factor *B* can be read from a graph published by Coker (2007). However, the values available for K_{OT} are only for mixers which inside diameters are in the range of about 0.15-0.3 meters. For the data available, the values for K_{OT} are between 21 and 41, mostly close to 30. (Coker, 2007) Therefore, an assumption that the K_{OT} values would be within similar range for larger mixers is made. To calculate the pressure drop in the mixer of demetallization process, the factor K_{OT} is estimated to be approximately 30. The manufacturer should be contacted in order to get more accurate data. The factor *B* is read from the graph and has a value of 1.95 (Coker, 2007). Therefore, the coefficient *K* is 58.5 which means the pressure drop in the mixer is 58.5 times the pressure drop in an empty pipe.

The pressure drop in an empty pipe due to friction can be calculated using Equation 22. The friction factor *f* is dependent on Reynolds number and relative roughness of the pipe. The relative roughness is the result of dividing the absolute pipe roughness by the pipe inside diameter. The absolute roughness of a commercial steel pipe is 0.046 mm and therefore, the relative roughness is $4.6 \cdot 10^{-5}$. As can be seen from Appendix 1, the friction factor is 0.0026. (Towler & Sinnott, 2013)

$$\Delta P = 8f\frac{L}{D_i}\frac{\rho u^2}{2} \tag{22}$$

where ΔP = pressure drop, Pa

f = friction factor

L = pipe length, m

D_i = pipe inside diameter, m

ρ = density of fluid, kg/m^3

u = fluid velocity, m/s

The pressure drop caused by the 180° elbows is estimated as a length of pipe that would cause the same pressure loss. Additionally, the pressure drop caused by the inlet and outlet of the mixer need to be taken into account when calculating the pressure drop in the mixer. The pressure drop in the elbows and in the inlet and outlet of the mixer are calculated using equivalent pipe diameters which are added to the length of the mixer in Equation 22. The number of equivalent pipe diameters for a 90° standard radius elbow is 30-40 and therefore, the number for a 180° standard radius elbow is estimated to be approximately 80. The number of equivalent pipe diameters for the inlet is 50 and for the outlet 25 for turbulent flow. (Towler & Sinnott, 2013)

The total length used in pressure drop calculation is 1203 m including the 20 m long mixing section. The mixing section consists of 17 m of straight pipe and one 180° elbow and therefore, the pressure drop in the 20 m long mixing section is calculated by multiplying the pressure drop in a 97 m long empty pipe with the coefficient *K*. Instead of adding the pressure drop caused by the inlet of the mixer to the mixing section, it is included in the pressure drop of the empty pipe.

Therefore,

$$\Delta P_{\text{mixing section}} = 874 \text{ Pa}$$

$$\Delta P_{\text{empty pipe}} = 170 \text{ Pa}$$

As a result, the total pressure drop in the static mixer is 1044 Pa.

Materials

The selection of materials of construction has a significant impact on the operability and economics of refining units. The 20 m long mixing section requires more resistant material than the empty pipe following the mixing section in order to minimize the corrosion caused by H_3PO_4. Although the concentration of phosphoric acid in the VGO stream during the mixing is extremely small, corrosion may still occur.

Carbon steel is the most common construction material in refineries. Every effort is made to use carbon steel because it is inexpensive, readily available and easily fabricated. It is generally used in hydrotreating units that operate at temperatures below 260 °C. (Garverick, 1994) Austenitic stainless steels and 20-type alloys such as 20Cb-3 are often applied in equipment where H_3PO_4 is being handled (Davis, 2000). As the amount of acid is relatively small, constructing the whole mixer using an expensive acid-resistant material would not be cost-efficient. A suitable option for the mixer could be to use austenitic stainless steel in the mixing section and carbon steel in the empty pipe. The austenitic stainless steel chosen for the mixing section is alloy 904L due to its superior corrosion resistant properties to phosphoric acid compared to conventional chrome nickel stainless steels (Fine Tubes, 2011). The construction material affects the wall thickness of the mixer which is calculated next in this chapter.

The static mixer needs to be well insulated to minimize heat losses and to keep the desired temperature. The insulation can be placed around each pipe individually or around a larger area including several pipes. The insulation needs to be easily removable when maintenance is required.

Wall thickness

The American Society of Mechanical Engineers (ASME) has a standard for pipeline transportation systems. The ASME Code for Pressure Piping is applied to determine the wall thickness of the static mixer. The wall thickness without corrosion allowance is calculated using Equation 23. (The American Society of Mechanical Engineers, 2012)

$$t = \frac{PD_o}{2S_yEF} \tag{23}$$

where t = wall thickness without corrosion allowance, mm

P = internal design gauge pressure, kPa

D_o = pipe outside diameter, mm

S_y = minimum yield strength of the pipe, kPa

E = weld joint factor

F = design factor based on nominal wall thickness

As only the inside diameter of the mixer is known, the outside diameter needs to be replaced in the equation. The outside diameter D_o equals the inside diameter D_i summed with two times the wall thickness t and two times the corrosion allowance c as can be seen in Figure 19.

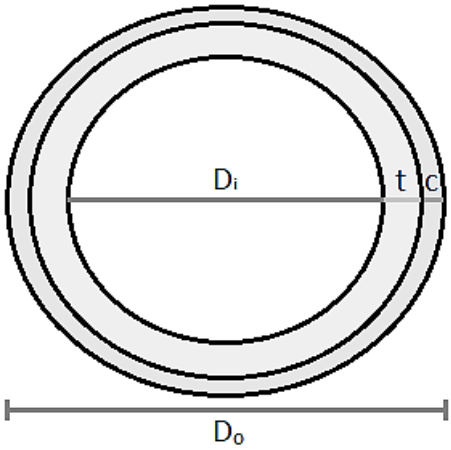

Figure 19. Cross-section of the mixer pipe; D_o outside diameter, D_i inside diameter, t wall thickness without corrosion allowance and c corrosion allowance.

Therefore, Equation 23 becomes

$$t = \frac{P(D_i + 2t + 2c)}{2S_yEF} = \frac{P(D_i + 2c)}{2S_yEF - 2P} \tag{24}$$

where D_i = pipe inside diameter, mm

c = corrosion allowance, mm

Based on the ASME Code, the minimum yield strength S_y of 904L welded pipe is 220 MPa. Carbon steel ASTM A53 grade A is used in the calculations of empty pipe and its minimum yield strength is 207 MPa. The weld joint factor E is 1.00 and the value of design factor F is 0.72 for both materials. (The American Society of Mechanical Engineers, 2012) According to Hurme (2008), a typical corrosion allowance for stainless steel is 1 mm. For carbon steel, a minimum corrosion allowance of 2.0 mm should be used when severe corrosion is not expected and an allowance of 4.0 mm when more severe corrosion is anticipated (Towler & Sinnott, 2013). Therefore, the mixing section has a corrosion allowance of 1 mm and the empty carbon steel pipe an allowance of 2 mm.

A recommended margin between the normal operating pressure and the design pressure is 10 % (Towler & Sinnott, 2013). As the operating pressure is 6.0 MPa in the mixer, the design pressure will be 6.6 MPa and design gauge pressure 6.5 MPa. As a result, the wall thicknesses *t* are

$$t_{\text{mixing section}} = 21.4 \text{ mm} \approx 21 \text{ mm}$$

$$t_{\text{empty pipe}} = 22.9 \text{ mm} \approx 23 \text{ mm}$$

The wall thicknesses with corrosion allowances are 22 mm for the mixing section and 25 mm for the empty pipe.

8.2.2 Decanter

The mixture of liquids leaving the mixer must be settled, coalesced and separated into its liquid phases. A decanter is possible equipment used for separating the oil phase from the aqueous phase. A horizontal cylindrical decanter is designed for the separation.

The aqueous phase consists of reaction products of the reaction between H_3PO_4 and metal impurities. The density of aqueous phase is estimated by using the densities of H_3PO_4 and pure solid metals. The densities and mass flow rates of the metal impurities reacting with H_3PO_4 are shown in Table 11. Average density is calculated applying Equation 18 and as a result, the average density of aqueous phase in the decanter is 1440 kg/m^3. Laboratory experiments are required to determine the density more accurately.

Table 11. Densities and mass flow rates of components present in aqueous phase.

Substance	Density (kg/m^3)	Mass flow rate in aqueous phase (kg/h)
Ni	8900*	0.288
V	6065*	0.207
Fe	7870*	0.066
H_3PO_4, 75 w-%	1350	7.000

*Source: (Yaws, 2011)

Dimensions of the decanter

In a decanter the velocity of continuous phase, in this case the oil phase, should be less than the settling velocity of the droplets of dispersed phase. The velocity of continuous phase is calculated using Equation 25 and Stokes' law is used to determine the settling velocity of the droplets (Equation 26). (Thakore & Bhatt, 2007; Towler & Sinnott, 2013)

$$u_c = \frac{V_c}{A_i} < u_d \tag{25}$$

where u_c = velocity of the continuous phase, m/s

V_c = volumetric flow rate of continuous phase, m^3/s

A_i = area of interface, m^2

u_d = settling velocity of the dispersed phase droplets, m/s

$$u_d = \frac{d_d^2 g(\rho_d - \rho_c)}{18\mu_c} \tag{26}$$

where d_d = droplet diameter, m

g = acceleration of gravity = 9.81 m/s^2

ρ_d = density of dispersed phase, kg/m^3

ρ_c = density of continuous phase, kg/m^3

μ_c = viscosity of continuous phase, Pa·s

The droplet size of 150 µm is often used for the sizing of a decanter because it is well below the droplet sizes normally found in decanter feeds. In a horizontal cylindrical decanter, the interfacial area A_i depends on the position of the interface and is calculated using Equation 27. Equation 28 is used to calculate the width of the interface needed to determine the interfacial area. The geometry of the horizontal decanter is presented in Figure 20. (Thakore & Bhatt, 2007; Towler & Sinnott, 2013)

$$A_i = wl \tag{27}$$

$$w = 2\sqrt{2rz - z^2} \tag{28}$$

where w = width of interface, m

l = length of decanter, m

r = radius of decanter, m

z = height of interface from the base of the vessel, m

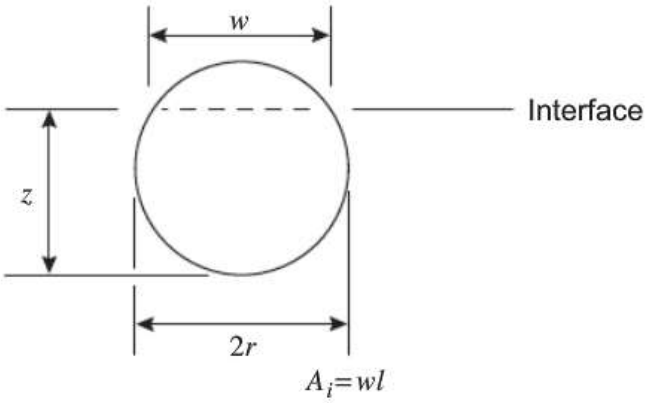

Figure 20. Geometry of horizontal decanter: *r* = radius of decanter, *w* = width of interface and *z* = height of the interface from the base of the vessel (Towler & Sinnott, 2013).

First, the settling velocity u_d is calculated using Equation 26 and subsequently, the minimum interfacial area A_i is obtained from Equation 25. The volumetric flow rate of the oil phase used in Equation 25 is the VGO feed flow rate subtracted by the flow rate of removed metal impurities.

$$\mathrm{u_d} = 3.58\ \mathrm{mm/s}$$

$$\mathrm{A_{i,min}} = \frac{\mathrm{V_c}}{\mathrm{u_d}} = \frac{\mathrm{m_c}}{\rho_c \mathrm{u_d}} = 30.64\ \mathrm{m^2}$$

As 7 kg/h of H_3PO_4 is mixed with 300 t/h of VGO, the amount of aqueous phase is extremely small compared to the oil phase. Due to the minuscule amount of aqueous phase, the position of the interface will be below the centre line of the decanter. The height of the liquid interface needs to be controlled accurately using a level instrument because of the small quantity of aqueous phase (Towler & Sinnott, 2013). The level instrument can control the height of the interphase by controlling the flow rate of aqueous phase leaving the decanter. In the design of the demetallization process, the position of the interphase is fixed at a height of $D_i/4$. Equation 28 becomes

$$w = 2\sqrt{D\frac{D}{4} - \left(\frac{D}{4}\right)^2} = \frac{D}{2}\sqrt{3}$$

For a horizontal decanter, the length is approximated to be four times the diameter (Thakore & Bhatt, 2007). Therefore, the minimum diameter of the decanter can be calculated using Equation 27.

$$A_{i,min} = \frac{D}{2}\sqrt{3} \cdot 4D = \sqrt{12}D_{min}^2 \rightarrow D_{min} = 2.97 \text{ m}$$

The minimum diameter required is 3.0 m and the length is 11.9 m. The large diameter causes the wall thickness of the decanter also to be large. The wall thickness is discussed later in this chapter.

The take-off locations can be determined by making a pressure balance. Neglecting the friction loss in the pipes, the pressure exerted by the combined height of the heavy and light liquid in the decanter must be balanced by the height of the heavy liquid in the take-off leg as can be seen in Figure 21. The pressure balance is presented in Equation 29. (Thakore & Bhatt, 2007; Towler & Sinnott, 2013)

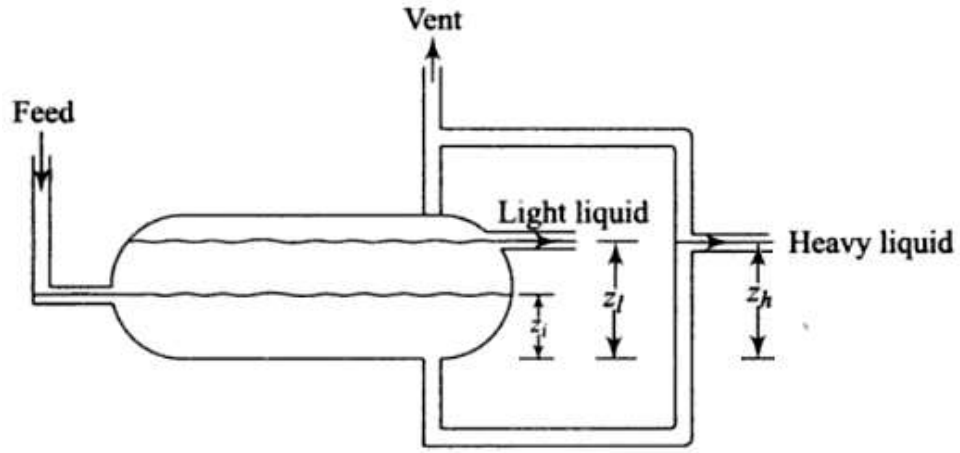

Figure 21. Location of light and heavy liquid take-offs; z_i height of the interface, z_l height of light liquid take-off and z_h height of heavy liquid take-off (Thakore & Bhatt, 2007).

$$(z_l - z_i)\rho_l g + z_i \rho_h g = z_h \rho_h g \quad (29)$$

where ρ_l = density of the light phase, kg/m^3

ρ_h = density of the heavy phase, kg/m^3

g = gravitational acceleration = 9.81 m/s^2

For a horizontal decanter, a good take-off height for the light phase is around 0.8 times the diameter (Thakore & Bhatt, 2007). As the height of the interface is one fourth of the diameter, the height of the heavy phase take-off can be calculated from the pressure balance.

$z_i = 0.74$ m

$z_l = 2.38$ m

$z_h = 1.61$ m

In order to minimize entrainment by the jet of liquid entering the decanter, the inlet velocity should be kept below 1 m/s. The inlet pipe diameter can be calculated using Equation 30. (Towler & Sinnott, 2013)

$$D_{\text{inlet pipe}} = \sqrt{\frac{4A}{\pi}} = \sqrt{\frac{4\left(\frac{m_h}{\rho_h} + \frac{m_l}{\rho_l}\right)}{\pi u}} \tag{30}$$

where A = cross-sectional area of inlet pipe, m^2

m_h = mass flow rate of heavy phase, kg/s

m_l = mass flow rate of light phase, kg/s

u = inlet velocity, m/s

Therefore,

$$D_{\text{inlet pipe}} = 0.374 \text{ m} \approx 0.4 \text{ m}$$

The inlet pipe diameter should be approximately 0.4 m in order to keep the inlet velocity below 1 m/s.

Materials

Carbon steel is the preferred construction material because it is inexpensive and readily available. As phosphoric acid reacts with the metal impurities in the mixer, corrosion due to H_3PO_4 does not occur in the decanter enabling the use of carbon steel. Therefore, the decanter is constructed of carbon steel without any protective linings.

Wall thickness

For design purposes, the pressure vessels are divided into two classes depending on the ratio of the wall thickness to vessel diameter. If the ratio is less than 1:10, the vessel is thin-walled and if it is above that value, the vessel is considered to be thick-walled. The decanter has a large diameter and therefore, the ratio will be less than 1:10 so it will be classified as a thin-walled vessel. (Towler & Sinnott, 2013)

The principal stresses affecting the wall of a vessel due to a pressure load are shown in Figure 22. As the wall is thin, the radial stress σ_3 will be small and can be neglected in comparison with the other stresses. The longitudinal stress σ_1 and the circumferential stress σ_2 can be taken as constant over the wall thickness. The majority of the vessels used in chemical industries are classified as thin-walled vessels. (Towler & Sinnott, 2013)

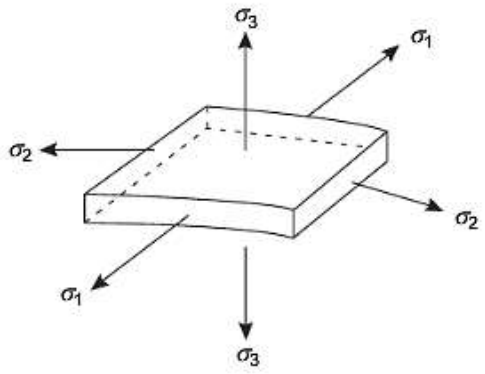

Figure 22. Principal stresses in a pressure vessel wall: σ_1 longitudinal stress, σ_2 circumferential stress and σ_3 radial stress (Towler & Sinnott, 2013).

The ASME Boiler & Pressure Vessel Code (BPVC) regulates the design and construction of boilers and pressure vessels. The minimum wall thicknesses due to longitudinal and circumferential stresses are calculated using Equations 31 and 32, respectively. The ASME BPVC specifies that the minimum wall thickness of a pressure vessel is the greater

value determined from these equations. (The American Society of Mechanical Engineers, 2010)

$$t = \frac{P_i D_i}{4SE + 0.8P_i} \tag{31}$$

$$t = \frac{P_i D_i}{2SE - 1.2P_i} \tag{32}$$

where t = vessel wall thickness, mm

P_i = internal pressure, kPa

D_i = inside diameter of vessel, mm

S = maximum allowable stress, kPa

E = joint efficiency

The operating pressure in decanter is close to the operating pressure in mixer because of the relatively small pressure drop in the mixer. Therefore, 6.6 MPa is also used as the design pressure for the decanter. Maximum allowable stresses for different materials are presented in ASME BPVC. Carbon steel SA/EN 10028-2 grade P355GH is used for the design of the decanter and the maximum allowable stress for that carbon steel is 137 MPa (The American Society of Mechanical Engineers, 2015). A good value for the joint efficiency *E* is 0.7 for preliminary design (Escoe, 2008).

Therefore, the minimum wall thickness due to longitudinal stress is

$$t = 51 \text{ mm}$$

and the minimum thickness due to circumferential stress is

$t = 108\ \text{mm}$

As a result, the minimum wall thickness of the decanter would be 108 mm. However, that great thickness implies that the mass of the decanter vessel will also be great. Applying two smaller decanters of 2.1 m diameter each in parallel would reduce the wall thickness to 75 mm. Similarly, using three decanters of 1.7 m diameter in parallel would further reduce the wall thickness to 61 mm. All these decanter configurations provide the same interfacial area for the separation. Applying several decanters reduces the wall thickness and the weight of the vessels but they require more land area.

A corrosion allowance is not included in the wall thicknesses calculated using Equations 31 and 32. The corrosion allowance should be based on experience with the material under similar conditions than the operating ones. The equal corrosion allowance of 2.0 mm is used in the decanter as in the empty carbon steel pipe of the mixer. The dimensions of different decanter configurations are summarized in Table 12.

Table 12. Dimensions of different decanter configurations.

Number of decanters	Diameter (m)	Length (m)	Wall thickness with 2 mm corrosion allowance (mm)
1	3.0	11.9	110
2	2.1	8.4	77
3	1.7	6.9	63

Decanter heads

Torispherical, ellipsoidal and hemispherical heads are commonly used for pressure vessels. Different head types are presented in Figure 23. The torispherical heads are usually used for pressures up to 20 bar, the ellipsoidal heads for pressures between 20

and 100 bar and the hemispherical heads for pressures above 100 bar. As the design pressure is 66 bar, the decanter is designed with ellipsoidal heads. (Hall, 2012)

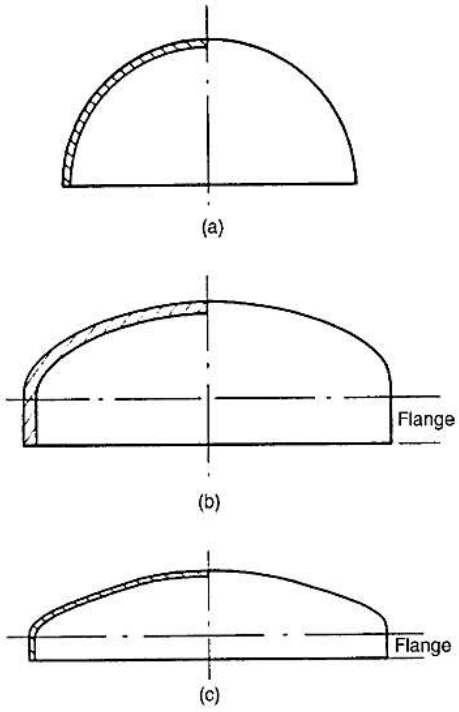

Figure 23. Pressure vessel heads: (a) hemispherical, (b) ellipsoidal and (c) torispherical (Towler & Sinnott, 2013).

The most standard ellipsoidal heads have a major-to-minor axis ratio of 2:1 (Towler & Sinnott, 2013). The depth of dish *a*, which can be seen in Figure 24, is the distance from a tangent line to the end of head. The tangent line is located in the beginning of the curvature of the head. Because the head includes a short straight section, the flange, the tangent-to-tangent distance of the vessel is greater than distance between the weld seams at the heads. The straight flange is roughly from 10 cm to 30 cm depending on diameter and thickness. The depth of dish *a* for an ellipsoidal vessel is one fourth of the inside diameter of the vessel. (Hall, 2012) The depth of dishes is presented in Table 13.

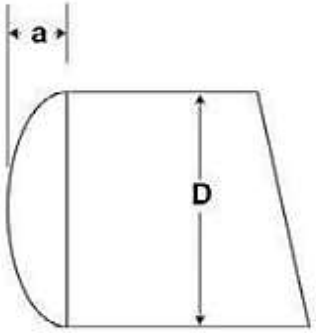

Figure 24. Depth of an ellipsoidal head; *a* is the distance from the tangent line to the end of head and *D* is the inside diameter of the vessel (Hall, 2012).

The wall thickness of the ellipsoidal head is calculated using Equation 33 (The American Society of Mechanical Engineers, 2010).

$$t = \frac{P_i D_i}{2SE - 0.2P_i} \tag{33}$$

where P_i = internal pressure, kPa

D_i = inside diameter of vessel, mm

S = maximum allowable stress, kPa

E = joint efficiency

If formed by pressing, the head has no joints and the joint efficiency *E* will be 1 (Towler & Sinnott, 2013). The head thicknesses of different decanter configurations are presented in Table 13.

Table 13. Depth of dishes and head thicknesses of different decanter configurations.

Number of decanters	Inside diameter (m)	Depth of dish (m)	Head thickness using Equation 33 (mm)
1	3.0	0.75	70
2	2.1	0.53	51
3	1.7	0.43	41

The head thickness of a decanter is rounded to the value of the shell wall thickness (Towler & Sinnott, 2013).

Decanter support

The decanter vessel must be supported. Generally, horizontal tanks and pressure vessels are supported on two vertical cradles called saddles. The use of more than two saddles is unnecessary and should be avoided as two saddles provide a high tolerance for soil settlement with no change in shell stresses. Usually, one end of the vessel is anchored and the other end sliding to enable the thermal expansion of the vessel. The saddle can be constructed of concrete or steel and it consists of various parts: the web, base plate, ribs and wear plate. (Moss & Basic, 2013)

The contact angle of vessel and wear plate should not be less than 120° and usually, it is between 120-150°. Typical saddle design dimensions for vessels with different diameters are shown in Figure 25 and Table 14. (Towler & Sinnott, 2013) The saddle designs listed in Table 14 present the closest values available to the decanter diameters of 3.0 m, 2.1 m and 1.7 m.

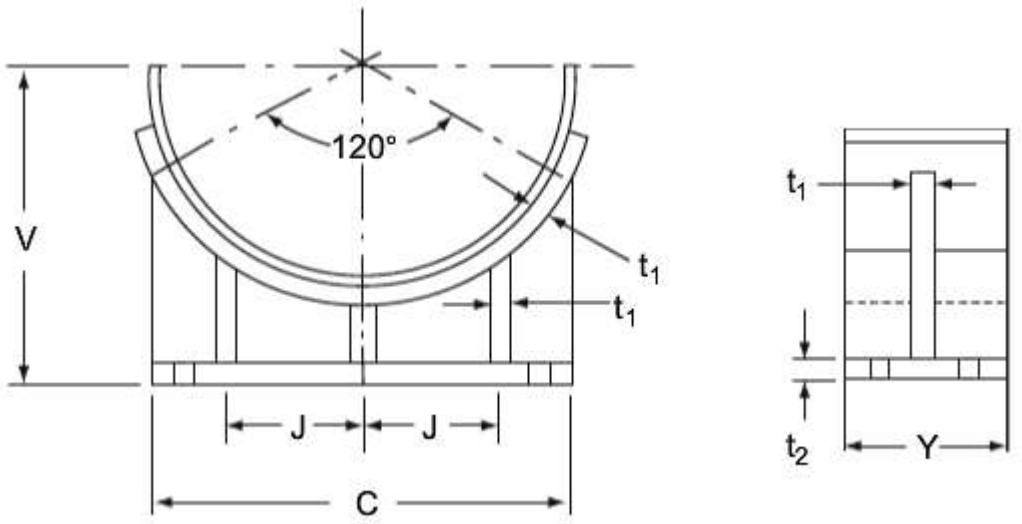

Figure 25. Dimensions of a saddle support: V distance from the bottom of the base plate to the center line of the vessel, J ribs spacing, C base plate length, Y base plate width, t_1 rib and web thickness, t_2 base plate thickness **(**Towler & Sinnott, 2013).

Table 14. Typical values for the saddle support design (Towler & Sinnott, 2013).

	Dimensions (m)				Dimensions (mm)	
Vessel diameter (m)	**V**	**J**	**C**	**Y**	**t_1**	**t_2**
1.6	0.98	0.350	1.41	0.20	10	12
1.8	1.08	0.405	1.59	0.20	10	12
2.0	1.18	0.450	1.77	0.20	10	12
2.2	1.28	0.520	1.95	0.23	12	16
3.0	1.68	0.665	2.64	0.25	12	16

8.2.3 Electrostatic coalescer

Alternative equipment for the separation of the phases is an electrostatic coalescer. The droplets of the aqueous phase may be so fine in diameter that they do not settle by gravity (Fahim *et al*., 2010). Moreover, the small amount of aqueous phase compared to the amount of oil phase can complicate the coalescing of the aqueous phase in the decanter.

Coalescing of the small water drops in oil can be done by using a high-voltage electrical field. When a non-conductive liquid containing dispersed conductive liquid is subjected to an electrical field, the conductive droplets are caused to combine. The electric field ionizes the water droplets which coalesce to produce larger drops that can be settled by gravity. Electrostatic coalescers are used for desalting crude oils. (Fahim *et al*., 2010)

A horizontal electrostatic coalescer is presented in Figure 26. The coalescer can contain two or more electrodes. One electrode is grounded to the vessel and the other suspended by insulators. An alternating current is used and the usual applied voltage ranges from 10 to 35 kV. The electrical charges of the electrodes reverse many times a second causing the water droplets to be in a rapid back-and-forth motion. The possibility of water droplets colliding with each other increases with greater motion of the droplets. The intensity of the electrostatic field is controlled by the applied voltage and the spacing of the electrodes. (Arnold & Stewart, 2008)

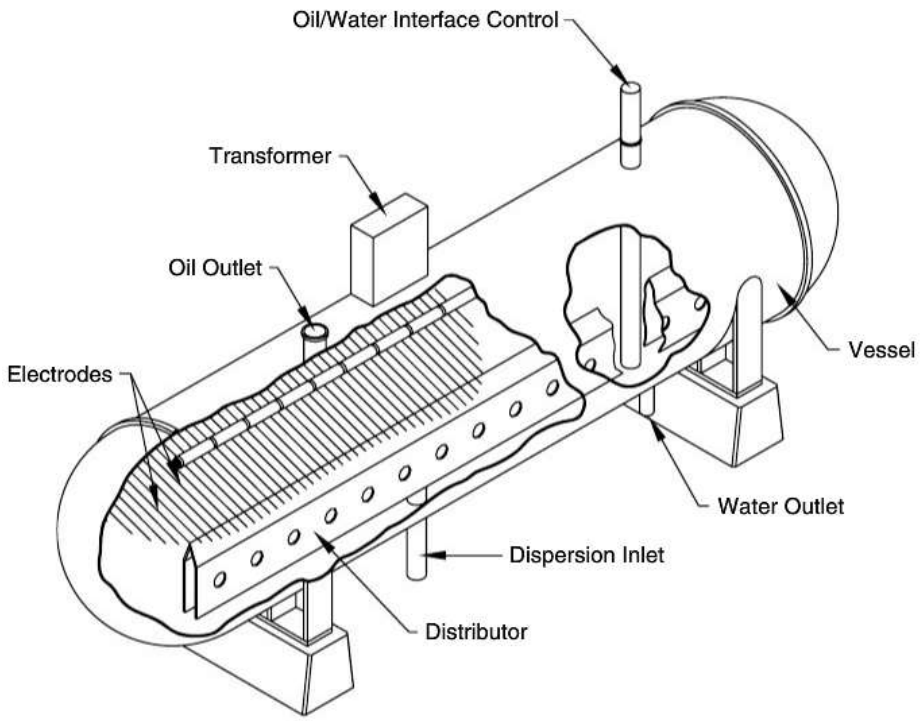

Figure 26. Cutaway of a horizontal electrostatic coalescer (Arnold & Stewart, 2008).

In the design of coalescer, preventing the water level from reaching the height of the electrodes is important. The salts present in the aqueous phase make it a very good conductor of electric currents. Therefore, a contact with the electrodes may short out the electrode grid or the transformer. The sizing of electrode grid area requires laboratory testing because the coalescence of droplets in an electric field is dependent on the characteristics of the specific mixture being treated. (Arnold & Stewart, 2008)

Coalescer vessels are sized for a certain volume flow per square meter of grid area. According to Arnold & Stewart (2008), procedures for designing electrostatic grids have not been published. As the coalescence of water droplets in an electric field is extremely dependent on the characteristics of the treated emulsion, it is unlikely that a general relationship of water droplet size to use in the settling equations can be developed.

8.2.4 Storage tank for phosphoric acid

Phosphoric acid requires a storage tank from where it is fed to the static mixer. Raw material storage sizing depends much on the logistics and economical delivery lots. Transporting H_3PO_4 in lots that are smaller than one full truck lot is relatively more expensive than transporting full truck lots. Therefore, the sizing of the storage tank is based on the capacity of a normal truck lot which is between 10 and 20 m^3 (American Society of Heating, Refrigerating and Air-Conditioning Engineers, Inc., 2012). Because the mass flow rate of H_3PO_4 is only 7 kg/h, a truck with 10 m^3 capacity can be used. To have some safety margin if the delivery is late or the consumption of the acid is greater than estimated, a two-week acid consumption with 7 kg/h flow rate is added to the volume of storage tank. Depending on the temperature of the acid, the total volume flow rate in 14 days is 1.5-1.7 m^3 and as a result, the storage tank would be 11.7 m^3. However, the tank should not be more than 85-90 % full (Hurme, 2008). Therefore, a tank of 14 m^3 would be sufficient.

The storage tank for H_3PO_4 requires a corrosion resistant material. The tank can be constructed of the same austenitic stainless steel that is used for the mixing section. The alloy 904L has good corrosion resistance to phosphoric acid (Fine Tubes, 2011).

A containment dike is applied to prevent major contamination to surrounding areas in case of leaks and spills. The dike must hold the content of the storage tank if a leak occurs. (Parisher & Rhea, 2012) The storage tanks are usually placed in a common area of the facility known as a tank farm. The tank farm should be placed between the loading and unloading facilities and the process units they serve. The area must be easily accessible in order to organize the unloading of the tanks practically and safely. (Towler & Sinnott, 2013)

8.3 Profitability

The costs related to the demetallization process are divided into investment and operating costs. The investment cost includes, for example, the costs of purchasing and installing the equipment while the operating costs result from purchasing the raw materials and changing the catalyst. In the end of this chapter, a sensitivity analysis is conducted and the profitability of the demetallization process is discussed.

8.3.1 Investment cost

The purchased equipment costs can be estimated in various ways. The best source of purchase costs is recent data on actual prices paid for similar equipment. Reliable information on equipment costs can also be found in professional cost engineering literature. In addition, different cost correlations and cost estimating software, for example Aspen Technology's Aspen ICARUS™ Technology, can be used for estimating chemical plant costs. (Towler & Sinnott, 2013)

Static mixer

The purchase costs of the mixing section and empty pipe are estimated separately. The sum of these costs forms the purchase cost of the static mixer.

ZAIN Technologies has published typical market prices of static mixers with diameters from 2 to 12 inches. The mixers are constructed from 316L stainless steel and they contain 3 or 6 helical mixing elements. (ZAIN Technologies, 2016) The prices are assumed to be updated to present values as they are taken from the company website. The price of a mixer, the diameter of which is 1 m, is roughly estimated by extrapolating the prices of 6-element mixers. The purchase cost of the mixing section in the demetallization process is estimated to be 5 times the price obtained by extrapolating as the mixing

section consists of 5 HEV mixing elements. As a result, the purchase cost of a mixer made of 316L stainless steel is US$125,000.

To estimate the purchase cost of the mixer constructed from 904L, a material cost factor is required. According to Steel Tank Institute/Steel Plate Fabricators Association, relative cost ratio between 904L and 316L is 2.16 (Steel Tank Institute/Steel Plate Fabricators Association, 2012). Therefore, the purchase cost of the mixing section made of 904L is US$270,000.

Finally, the U.S. dollars are converted into euros by applying the currency rate of U.S. dollar on 17th of February 2016. On that date, one euro was worth 1.11332 U.S. dollars (Kauppalehti, 2016). Therefore, 270 k$ equals 243 k€.

The cost of the empty pipe is estimated based on its weight. The weight of the empty pipe is calculated by multiplying the volume of carbon steel in the empty pipe by its density. The density of carbon steel used in the calculations is 7800 kg/m^3. The world carbon steel price was taken from the tables of Management Engineering & Production Services. The price in 2015 was approximately 500 US$/ton (Management Engineering & Production Services, 2016). The previously used currency rate of U.S. dollar is applied to convert the cost in euros. The purchase cost of the carbon steel pipe is estimated to be twice the material cost. The cost of the empty carbon steel pipe is presented in Table 15.

Table 15. Cost of the empty carbon steel pipe required for the static mixer.

	Inside diameter (m)	**Length (m)**	**Wall thickness (mm)**	**Weight (kg)**	**Cost of carbon steel (k$)**	**Cost of carbon steel (k€)**	**Purchase cost of pipe (k€)**
Carbon steel pipe	1	148	25	92930	46.5	41.7	83.5

The total purchase cost of the static mixer is the sum of the costs of mixing section and the empty carbon steel pipe. As can be seen in Table 16, the purchase cost of static mixer is 326.5 k€. The installed cost of the mixer is preliminarily estimated to be three times the purchase cost. Therefore, the cost of installed static mixer is 980 k€.

Table 16. Purchase cost of static mixer.

Equipment	Purchase cost (k€)
Mixing section	243
Empty carbon steel pipe	83.5
Static mixer	326.5

Decanter

The purchase cost of a horizontal carbon steel pressure vessel can be calculated using Equation 34 which is based on the weight of the shell and two 2:1 ellipsoidal heads. The purchase cost is in year 2000 basis and includes an allowance for platform, ladders and manholes. (Seider *et al*., 2004)

$$C_p = \exp(8.717 - 0.2330 \ln W + 0.04333(\ln W)^2) + 1580 D_i^{0.20294} \quad (34)$$

where C_p = purchase cost of horizontal carbon steel pressure vessel, $

W = weight of shell and two heads, lb

D_i = inside diameter of vessel, ft

The costs are calculated for three different decanter configurations: one decanter of 3.0 m diameter, two decanters of 2.1 m diameter each and three decanters of 1.7 m diameter each. The weight of vessel shells is presented in Table 17.

Table 17. Shell weight of decanters.

Number of decanters	Diameter (m)	Length (m)	Wall thickness (mm)	Volume of carbon steel in one decanter (m^3)	Shell weight of one decanter (kg)
1	3.0	11.9	110	12.7	98800
2	2.1	8.4	77	4.4	34600
3	1.7	6.9	63	2.4	18900

The weight of a vessel head can be accurately determined by calculating the volume of a circular blank. The blank diameter of a 2:1 ellipsoidal head is calculated using Equation 35. (Escoe, 2008)

$$D_b = 1.22D_i + 2(S.F.) + t \quad (35)$$

where D_b = blank diameter, m

D_i = inside diameter, m

S.F. = straight flange of head, m

t = head thickness, m

For the straight flange a value of 0.2 m is used in the preliminary design. The weight of the vessel head is obtained by multiplying the volume of the circular blank with the density of carbon steel. The results are shown in Table 18.

Table 18. Vessel head weights and the total weight of shells and heads.

Number of decanters	Inside diameter (m)	Straight flange of head (m)	Head thickness (mm)	Blank diameter (m)	Weight of one head (kg)
1	3.0	0.2	110	4.14	11530
2	2.1	0.2	77	3.04	4360
3	1.7	0.2	63	2.56	2520

To calculate the purchase cost of the decanters, the diameters need to be converted into feet and the weights into pounds. The purchase costs of different decanter configurations are shown in Table 19.

Table 19. Total purchase cost of decanters in U.S. dollars in 2000.

Number of decanters	D_i(m)	D_i(ft)	Weight of one shell and two heads (kg)	Weight of one shell and two heads (lb)	Purchase cost of one decanter in 2000 ($)	Total purchase cost in 2000 ($)
1	3.0	9.8	121890	268720	292000	292000
2	2.1	6.9	43300	95450	128100	256200
3	1.7	5.6	23900	52680	83500	250500

The costs calculated using Equation 34 are in year 2000 basis. To update the costs to present value a chemical engineering plant cost index (CEPCI) is applied. The CEPCI in 2000 was 394. (Seider *et al*., 2004) The most recent CEPCI available is for April 2015 when the value was 562.9 (Chemical Engineering, 2015). Therefore, the costs in April 2015 can be calculated using Equation 36 (Towler & Sinnott, 2013).

$$C_{\text{April 2015}} = C_{2000} \frac{\text{CEPCI}_{\text{April 2015}}}{\text{CEPCI}_{2000}} \tag{36}$$

The purchase costs in April 2015 can be seen in Table 20. The currency is converted into euros using the same currency rate as previously. The cost of an installed carbon steel pressure vessel can be estimated by multiplying the purchase cost by a factor of 4.1. The installed cost includes the installation of equipment, cost of site preparations, foundations, structures, piping, engineering, fee of contractor and supervision. (Hurme, 2008)

Table 20. Total purchase and installed cost of decanters in 2015.

Number of decanters	Total purchase cost in 2015 (k$)	Total purchase cost in 2015 (k€)	Total installed cost of decanters in 2015 (k€)
1	417	375	1537
2	366	329	1348
3	358	322	1318

Applying three smaller decanters has the lowest purchase cost. However, the difference in purchase costs between two decanters and three decanters is not great. Even though the decanters are smaller, applying three decanters will require more space than one larger decanter. Furthermore, more piping is needed as the VGO stream is divided into three decanters and after combined back together before feeding it to the reactor. The large decanter weights more than the other decanter configurations and therefore, it requires stronger and more durable foundations that can withstand the combined weight of the decanter and the VGO stream.

Due to the lowest purchase cost, three decanters are used in the sensitivity analysis which is conducted in chapter 8.3.3. In addition, if three decanters are applied in parallel, the process would not need to be shut down if problems occurred in one of the decanters. By reducing the flow rate, one decanter could be under maintenance while the other two remain working.

8.3.2 Operating costs

The operating costs of demetallization process are discussed in this chapter. The operating costs consist of the purchase costs of raw materials and the cost of changing the catalysts.

Purchase cost of VGO and phosphoric acid

If a VGO feed with 10 ppm of metal impurities could be used, the purchase cost would be lower compared to the cleaner VGO feed currently utilized in the refinery. Currently, VGO with high impurity levels is approximately 12 US$/ton cheaper than the cleaner VGO. However, the same VGO feed is used in both cases 1 and 2 so the purchase cost of VGO will not affect the comparison of these two cases.

Based on a market analysis report of PotashCorp, the price of phosphoric acid was 600-1100 US$/ton between January 2010 and January 2014. The average price was approximately 800 US$/ton. (PotashCorp, 2014)

Cost of changing the catalyst

The amount of metal impurities accumulating on the guard bed catalyst depends on the phase separation in the decanter or electrostatic coalescer. As the amount of the aqueous phase is extremely small compared to the oil phase, the aqueous phase might be so dispersed that the coalescence and separation into two phases will not occur completely. As a result, a part of the aqueous phase flows into the HDS reactors with the oil phase.

The catalyst lifetime is calculated assuming that the phases are separated perfectly. However, depending on the efficiency of the separation method the catalyst lifetime may be slightly shorter. The most of the metal impurities are present in the oil phase despite the use of phosphoric acid and therefore, the small possible part of aqueous phase

entering the reactors will not significantly reduce the catalyst lifetime. The amount of accumulated metal impurities in the guard bed catalyst is presented in Table 21.

Table 21. Accumulation of metal impurities in guard bed after demetallization.

			Accumulation of impurities in the guard bed (kg)						
Week	Feed stream (t/h)	Feed stream (t/wk)	As	Ca	Fe	Na	V	Ni	Total
1	300	50400	1.3	11.3	9.8	25.2	29.1	25.7	102
2	300	50400	2.5	22.7	19.7	50.4	58.2	51.4	205
3	300	50400	3.8	34.0	29.5	75.6	87.3	77.1	307
4	300	50400	5.0	45.4	39.3	100.8	116.4	102.8	410
5	300	50400	6.3	56.7	49.1	126.0	145.5	128.5	512
6	300	50400	7.6	68.0	59.0	151.2	174.6	154.2	615
7	300	50400	8.8	79.4	68.8	176.4	203.7	179.9	717
8	300	50400	10.1	90.7	78.6	201.6	232.8	205.6	820
9	300	50400	11.3	102.1	88.5	226.8	262.0	231.3	922
10	300	50400	12.6	113.4	98.3	252.0	291.1	257.0	1024
11	300	50400	13.9	124.7	108.1	277.2	320.2	282.7	1127
12	300	50400	15.1	136.1	117.9	302.4	349.3	308.4	1229

As discussed earlier, the adsorption capacity of the guard bed is 1.2 tons of metal impurities. The capacity is full during the week 12. Using the research data of Neste, the HDS catalyst will be deactivated already during week 10 and therefore, the catalyst lifetime is 9 weeks. Applying the demetallization process extends the catalyst lifetime only by one week. The reason why the catalyst lifetime does not extend more is that phosphoric acid reduces only the concentration of nickel, vanadium and iron. Moreover, the removal rates of nickel, vanadium and iron are fairly low. The rest of the impurities continue to deactivate the catalyst as their amount is not affected by phosphoric acid.

The costs of a process shutdown in Neste cannot be published in the thesis. Therefore, the cost of changing the catalysts during one process shutdown is calculated using costs published by Gorra *et al.* (1993). According to their article, one shutdown lasted 10 days and the lost profit was 39 US$/ton. The average catalyst handling cost was US$61,000

and the catalyst price 5 US$/kg. (Gorra *et al*., 1993) The labour costs were not published but to the best of knowledge, the labour costs form only a small part of the total costs. Especially compared to the lost profit, the labour costs are relatively low.

Costs of changing the catalyst during one shutdown are presented in Table 22. The costs in 1993 are converted into current values by taking into account the inflation. The mean value of inflation in the United States between 1993 and 2016 is approximately 2.2 % (Trading Economics, 2016). The previously used currency rate of U.S. dollar is applied for the conversion into euros.

Table 22. Costs of changing the catalysts during one process shutdown.

Costs of changing the catalyst	**In 1993 (k$)**	**In 2016 (k$)**	**In 2016 (k€)**
Lost production	2808	4632	4161
Catalyst handling cost	61	101	90
Catalyst price	1000	1650	1482
Total cost	3869	6383	5733

Based on the article by Gorra *et al*. (1993), the cost of one process shutdown is 5.7 M€. The cost of changing the catalyst during one shutdown is the same for case 1. Compared to the investment costs, the costs caused by the shutdowns are significantly greater. A sensitivity analysis is conducted in the following chapter and the impacts of different parameters on the profitability are discussed.

8.3.3 Sensitivity analysis

A sensitivity analysis is a tool for examining the effects of uncertainties in the forecasts on the viability of a project. The purpose is to identify the parameters that have a significant impact on the project viability and investigate the effect by varying each parameter individually. The result of the sensitivity analysis is often presented as a plot

of net present value (NPV) versus the parameter studied. The NPV is strongly dependent on the interest rate and the time period studied. (Towler & Sinnott, 2013) For the demetallization process, the NPV is calculated for a 10-year operating period with a 15 % interest rate. The parameters studied in the sensitivity analysis are the number of shutdowns, investment cost and purchase cost difference between low-quality and cleaner VGO.

For the phase separation, three decanters are applied. Therefore, the investment costs used in the sensitivity analysis consist of the installed costs of static mixer and three decanters. The investment cost is 2298 k€.

As the HDS catalyst lifetime is 9 weeks and each shutdown lasts 10 days, 5 catalyst change shutdowns are needed during each year. As a result, the process is under operation 45 weeks per year. The possibility to utilize low-quality VGO with high impurity levels saves US$12 per ton in VGO purchase costs. The annual savings due to cheaper VGO are shown in Table 23. The savings are equal each year during the 10-year period.

Table 23. Annual savings due to the use of cheaper VGO.

Period	Number of operating weeks	Processed VGO (tons)	Savings due to cheaper VGO (k$)	Savings due to cheaper VGO (k€)
1 year	45	2268000	27216	24446

The annual costs of purchasing H_3PO_4 and changing the catalyst are presented in Table 24. In the calculations, 800 US$/ton is used as the purchase price for the acid. The total annual cash flow is calculated by subtracting the H_3PO_4 purchase costs and catalyst changing costs from the savings shown in Table 23. The total cash flow of each year is then discounted in order to obtain the present value. The present values of the total cash flows are presented in Table 25 and in Figure 27. The investment in the equipment occurs in year 0.

Table 24. Annual cost of purchasing H_3PO_4 and changing the catalysts.

Period	Number of operating weeks	Number of shutdowns	Amount of H_3PO_4 used (tons)	Cost of purchasing H_3PO_4 (k$)	Cost of purchasing H_3PO_4 (k€)	Cost of changing the catalysts (k€)
1 year	45	5	53	42	38	28665

Table 25. Present value of total cash flow.

Year	Discounting factor when 15 % interest rate	Total cash flow (k€)	Present value of total cash flow (k€)
0	1.0000	-2298	-2298
1	0.8696	-4257	-3702
2	0.7561	-4257	-3219
3	0.6575	-4257	-2799
4	0.5718	-4257	-2434
5	0.4972	-4257	-2117
6	0.4323	-4257	-1840
7	0.3759	-4257	-1600
8	0.3269	-4257	-1392
9	0.2843	-4257	-1210
10	0.2472	-4257	-1052

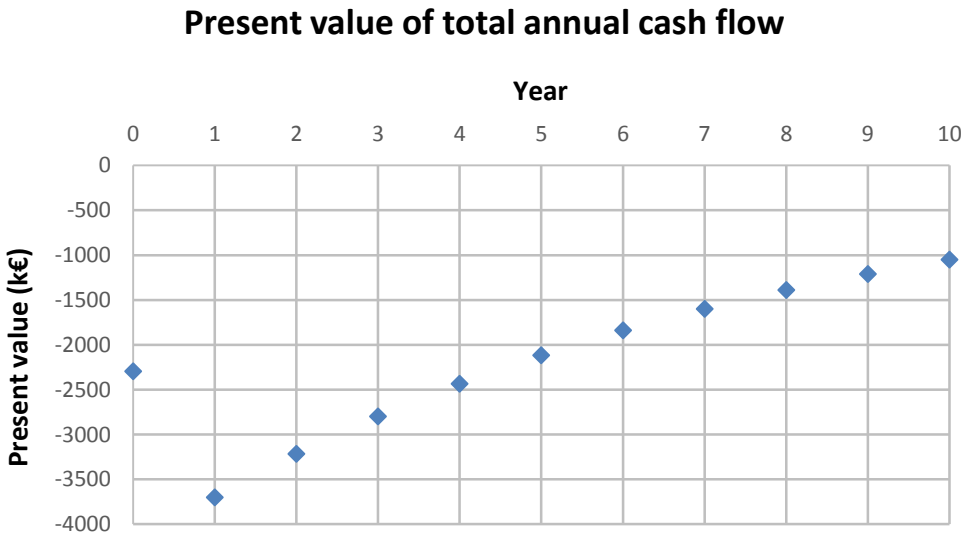

Figure 27. Present value of total annual cash flow.

The NPV is the sum of the present values of the cash flow and therefore, the NPV of the 10-year period in the demetallization process is -23664 k€. As the NPV is negative, investing in the demetallization process is not a cost-effective option with the current prices and costs.

The process viability depends on the number of shutdowns, investment cost and purchase cost difference between low-quality and cleaner VGO. To study the effects of these parameters on the process viability, each of the parameters are individually varied in the range from -50 % to +50 %. The results are presented as a plot of NPV versus change in parameter value and can be seen in Figure 28.

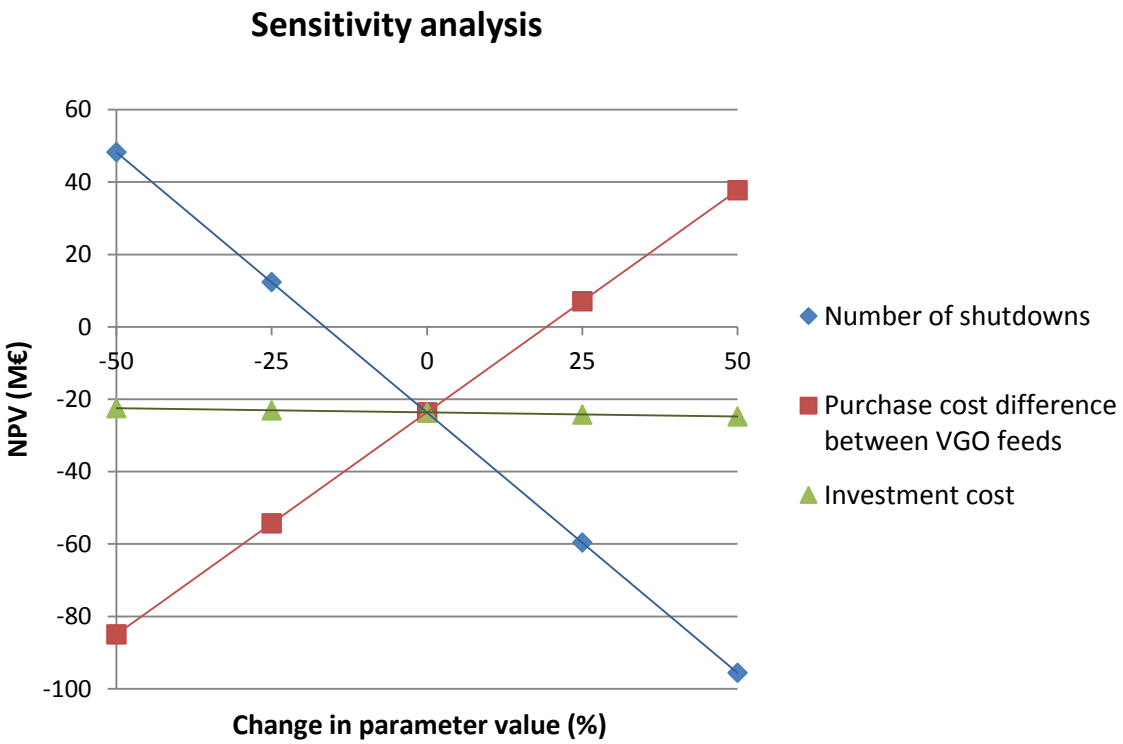

Figure 28. Sensitivity analysis.

From Figure 28 can be seen that the number of shutdowns and the difference in VGO purchase costs have the strongest impact on the viability of the process. The changes in investment costs do not significantly affect the NPV. The NPV becomes positive if the number of shutdowns is reduced at least by 17 % or the difference in VGO purchase costs increases by 20 % or more. These values are summarized in Table 26. In order to reduce the number of shutdowns by 17 %, the nickel, vanadium and iron levels must be reduced by additional 45 %. As a result, the required removal rates for nickel, vanadium and iron are 63 w%, 58 w% and 57 w%, respectively.

Table 26. Changes in parameter value that convert the NPV positive.

Parameter	Current value	Value which converts NPV positive	Change compared to current value
Number of shutdowns during 1 year	5	4.15	-17 %
Purchase cost difference between low-quality and cleaner VGO ($/ton)	12	14.4	+20 %

8.4 Safety

Safety issues form an important part of process design. If the designed process is not safe to operate, it is not viable. All safety risks must be eliminated or minimized to an acceptable level.

Overpressure is one of the most serious hazards in a chemical plant. Overpressure will occur when mass, moles or energy accumulate in a contained space with a restricted outflow. For example blocked outlet, valve failure or external fire can be a cause of overpressure in the demetallization process. To ensure that the pressure inside a vessel cannot rise to an unsafe level, pressure relief devices must be installed. Pressure relief devices are an essential requirement for the safe use of pressure vessels as they provide

a safe means of relieving overpressure. (Towler & Sinnott, 2013) Therefore, each decanter must contain a pressure relief device.

Generally, high temperatures can arise from the loss of control of reactors and heaters and from external fires (Towler & Sinnott, 2013). As the amount of metal impurities in the VGO is extremely small, the heat of reaction will not significantly affect the temperature of the VGO stream. Therefore, the more probable cause of high temperature in the demetallization process is an external fire. The safety of the whole chemical plant and the design of the layout contribute to minimizing the probability of external fires. Secure water supplies for firefighting must be available and at least two escape routes provided from each level in process buildings (Towler & Sinnott, 2013).

In addition to high temperatures, also too low temperatures cause problems in operating the process. Low temperatures will increase the viscosity of VGO and therefore, restrict its flow through the pipes and equipment. If problems occur in maintaining the temperature of the VGO feed storage tank in the right level, the VGO becomes too viscous to flow causing blockages.

The reactions occurring in the mixer need to be studied in order to find the optimum reaction conditions and to identify side reactions. Reaction products can be hazardous and require special handling which makes their identification important.

The probability of leaks should be minimized by careful equipment design. The corrosion can be minimized by selecting suitable materials and operating conditions. The storage tank of H_3PO_4, the pipeline feeding the acid to the mixer and the mixing section of the static mixer have the most corrosive condition. The flow rate of H_3PO_4 into the mixer must be controlled in relation to the VGO stream. If feeding of VGO is stopped due to problems in the process, a flow rate controller must stop the acid feed in order to not waste acid and to avoid corrosion problems in the mixer and decanters. Adequate maintenance procedures secure that the equipment stay in good condition during

operation. In addition, the plant needs to be supplied with drainage and sewer systems which collect the possible runoff, firefighting water and rainwater for waste treatment (Towler & Sinnott, 2013).

The sparking of electrical equipment, such as motors, is a potential source of ignition (Towler & Sinnott, 2013). As the mixing is obtained without a moving agitator, the static mixer has no motor. Therefore, the process contains one ignition source less. All electrical equipment must be grounded adequately (Towler & Sinnott, 2013).

If three decanters were applied in parallel, the process would not need to be shut down if problems occurred in one of the decanters. By reducing the flow rate, one decanter could be under maintenance while the other two are working. The static mixer does not have a duplicate system. Because the mixer is a pipe which does not contain moving parts, it requires only little maintenance and therefore, applying a duplicate system is unnecessary. The maintenance required due to fouling can be performed during planned process shutdowns. If sudden problems in operating the process occur and require a process shutdown, there must be secure means of controlling the process into a stable and safe state.

The aqueous phase separated in the decanter or electrostatic coalescer must be treated. The amount of aqueous phase to treat should be reduced to the possible minimum in order to minimize the costs of waste treatment. To minimize the amount of aqueous phase, the amount and quality of phosphoric acid fed to the mixer need to be optimized by performing laboratory experiments. The refinery has a wastewater treatment plant and the applicability of already existing treatment processes should be studied. If the aqueous phase cannot be treated utilizing own processes, purchasing the treatment from a specialized waste treatment company can be the best option.

Although the demetallization process produces waste in the form of aqueous waste stream, the catalyst waste could be reduced as the catalysts are changed less frequently.

If the demetallization process efficiently reduced the amount of metal impurities in the VGO, the amount of catalyst waste and the cost of treating it would significantly decrease. Moreover, the costs of purchasing new fresh catalyst would also decrease.

9 Discussion

The HDS catalyst deactivates fast in both cases 1 and 2. Due to the rapid deactivation, a pretreatment process is required if a VGO feed with 10 ppm of metal impurities is used. However, the demetallization process utilizing phosphoric acid does not remove sufficiently metal impurities based on the experimental data available. More experimental data would be required to optimize the process conditions and to determine the actual removal rates of metal impurities in the demetallization process.

The average cost per year caused by the shutdowns is presented in Table 27. In both cases, the reactors are packed with catalysts before the operation is started. The lost profit forms the largest share of the shutdown costs.

Table 27. Average annual cost due to the catalyst change shutdowns.

Process	Number of shutdowns during one year	Total annual cost of changing the catalyst (M€)
Case 1: without demetallization	5.5	31.5
Case 2: with demetallization	5	28.7

The costs caused by the shutdowns are enormous making the investment cost of the demetallization process a substantially small part of the total costs. Adding the demetallization process increases both the amount of equipment and the maintenance costs related to equipment. However, as the static mixer and decanter do not include

moving parts, the maintenance costs of demetallization equipment are relatively low compared to the maintenance costs of other equipment in the HDS process.

According to the sensitivity analysis in chapter 8.3.3, the number of shutdowns must decrease or the difference in purchase costs between low-quality and cleaner VGO must increase in order to make the demetallization process profitable. However, achieving sufficiently high removal rates with phosphoric acid to make the process feasible is improbable based on the available data. Moreover, the degree to which the phases can be separated needs to be studied. As the amount of acid is minuscule compared to the amount of VGO, separating the dispersed phase in a decanter may be problematic. If the phases are not completely separated, more impurities enter the HDS reactors shortening the catalyst lifetime.

10 Conclusions

The aim of this thesis was to study possible impurity removal methods for VGO prior to the HDS process. An impurity removal pretreatment could enable the use of cheaper, poor-quality VGO which has high impurity levels.

In the literature part of this thesis, impurities in VGO and different impurity removal methods were discussed. Based on the advantages and disadvantages of the methods, demetallization process utilizing phosphoric acid was chosen to be preliminarily designed in the applied part.

VGO feed with 10 ppm of metal impurities was used in the HDS process. Without the demetallization process, the HDS catalyst lifetime was only 8 weeks. Due to the rapid deactivation, a pretreatment process is required if a VGO feed with 10 ppm of metal impurities is used. Integrating the demetallization process into the HDS extended the catalyst lifetime by one week resulting in a catalyst lifetime of 9 weeks. The catalyst

changing shutdowns would occur 5 times each year. The demetallization process utilizing phosphoric acid does not remove sufficiently metal impurities based on the experimental data available.

The cost of one process shutdown was 5733 k€. The costs caused by the shutdowns were enormous mainly due to lost profit. The investment cost of the demetallization process was 2298 k€ which formed a relatively small part of the total costs as the shutdowns occurred frequently. The investment cost did not affect the profitability of the process significantly. However, by reducing the number of shutdowns by 17 % or increasing the purchase cost difference between low-quality and cleaner VGO by 20 %, the net present value of the demetallization became positive. Based on the available data, achieving sufficiently high removal rates with phosphoric acid to make the process feasible is improbable.

More experimental data is required to determine the optimal operating conditions and the actual removal rates. Also more experiments are needed to study if the phase separation is possible as the amount of H_3PO_4 is extremely small compared to the amount of VGO.

Bibliography

Abbas, S., Maqsood, Z. & Ali, M., The Demetallization of Residual Fuel Oil and Petroleum Residue, *Petroleum Science and Technology* **28** (2010) 1770-1777.

Adams, C., Ellert, H., Kimberlin Jr., C. & Hamner, G., Demetallization with hydrofluoric acid, Patent No. US3203892 A, 1965.

Admix, Sizing the Admixer Static Mixer and Sanitary Static Blender, http://www.admix.com/pdfs/admixer-tech102.pdf, Accessed 14 March 2016.

Airgas, Safety Data Sheet, Hydrogen Fluoride, https://www.airgas.com/msds/001077.pdf, Accessed 13 November 2015.

Ali, M. & Abbas, S., A review of methods for the demetallization of residual fuel oils, *Fuel Processing Technology* **87** (2006) 573-584.

American Society of Heating, Refrigerating and Air-Conditioning Engineers, Inc., *ASHRAE Handbook - Heating, Ventilating, and Air-Conditioning Systems and Equipment*, American Society of Heating, Refrigerating and Air-Conditioning Engineers, Inc., 2012, p. 31.14.

Arnold, K. & Stewart, M., *Surface Production Operations - Design of Oil Handling Systems and Facilities, Volume 1*, Elsevier, 2008, pp. 377-383.

Bahadori, A., *Essentials of Coating, Painting, and Lining for the Oil, Gas, and Petrochemical Industries*, Elsevier, 2015, pp. 297-300.

Bertoncini, F., Courtiade-Tholance, M. & Thiébaut, D., *Gas Chromatography and 2D-Gas Chroma for Petroleum Industry - The Race for Selectivity*, Editions Technip, 2013, pp. 2-3.

Bonné, R., van Steenderen, P. & Moulijn, J., Hydrogenation of nickel and vanadyl tetraphenylporphyrin in absence of a catalyst: A kinetic study. *Applied Catalysis A: General* **206** (2001) 171-181.

Bröll, D., Kaul, C., Krämer, A., Krammer, P., Richter, T., Jung, M., Vogel, H. & Zehner, P., Chemistry in Supercritical Water. *Angewandte Chemie (International ed.)* **38** (1999) 2998-3014.

Chainet, F., Courtiade, M., Lienemann, C.-P., Ponthus, J. & Donard, O., Silicon speciation by gas chromatography coupled to mass spectrometry in gasolines. *Journal of Chromatography A* **1218** (2011) 9269-9278.

Chainet, F., Le Meur, L., Lienemann, C.-P., Ponthus, J., Courtiade, M. & Donard, O., Characterization of silicon species issued from PDMS degradation under thermal cracking of hydrocarbons: Part 1 – Gas samples analysis by gas chromatography-time of flight mass spectrometry. *Fuel* **111** (2013) 519-527.

Chemical Engineering, Plant Cost Index, http://www.chemengonline.com/pci, Accessed 17 February 2016.

Coker, A., *Modeling of Chemical Kinetics and Reactor* Design, Elsevier, 2001, pp. 597-600.

Coker, A., *Ludwig's Applied Process Design for Chemical and Petrochemical Plants, Volume 1*, Elsevier, 2007, pp. xxv, 506-514.

Couper, J., Penney, W., Fair, J. & Walas, S., *Chemical Process Equipment - Selection and Design*, 3rd edition, Elsevier, 2012, p. 305.

Davis, J., *Corrosion - Understanding the Basics*, ASM International, 2000, pp. 220-225.

Dechaine, G. & Gray, M., Chemistry and Association of Vanadium Compounds in Heavy Oil and Bitumen, and Implications for Their Selective Removal, *Energy Fuels* **24** (2010) 2795-2808.

Eidem, P., Reducing the metals content of petroleum feedstocks, Patent No. US4752382 A, 1988.

Escoe, A., *Pressure Vessel and Stacks Field Repair Manual*, Elsevier, 2008, pp. 11-14, 25-26.

European Parliament & Council of the European Union, *Directive 2009/30/EC of the European Parliament and of the Council*, 2009.

Fahim, M., Al-Sahhaf, T. & Elkilani, A., *Fundamentals of Petroleum Refining*, Butterworth-Heinemann, 2010, pp. 19-20, 76-82, 155, 167-169, 327-328.

Fine Tubes, Alloy 904L (UNS N08904). http://www.finetubes.co.uk/uploads/docs/Alloy_904L.pdf, Accessed 18 March 2016.

Furimsky, E. & Massoth, F., Deactivation of hydroprocessing catalysts, *Catalysis Today* **52** (1999) 381-495.

Furimsky, E. & Massoth, F., Hydrodenitrogenation of Petroleum, *Catalysis Reviews* **47** (2005) 297-489.

Gaile, A., Semenov, L., Varshavskii, M., Erzhenkov, A., Koldobskaya, L. & Kaifadzhyan, E., Extraction Refining of Light Vacuum Gas Oil, *Russian Journal of Applied Chemistry* **74** (2001) 325-329.

Garverick, L., *Corrosion in the Petrochemical Industry*, ASM International, 1994, pp. 321-329.

Gawel, I., Bociarska, D. & Biskupski, P., Effect of asphaltenes on hydroprocessing of heavy oils and residua, *Applied Catalysis A: General* **295** (2005) 89-94.

Gerrard, M., *Guide to Capital Cost Estimating*, IChemE, 2000, p. 85.

Gorra, F., Scribano, G., Christensen, P., Vibeke Andersen, K. & Gaetano Corsaro, O., New catalyst, improved presulfiding result in 4+ year hydrotreater run, *Oil & Gas Journal* **91** (1993) 39-43.

Hall, S., *Rules of Thumb for Chemical Engineers*, Elsevier, 2012, pp. 150-151, 163.

Hurme, M., *Process Design Manual*, 2008, 107 p.

Jechura, J., Refinery Feedstocks & Products - Properties & Specifications. http://inside.mines.edu/~jjechura/Refining/02_Feedstocks_&_Products.pdf, Accessed 4 February 2016.

Jones, D. & Pujadó, P., *Handbook of Petroleum Processing*, Springer, 2006, pp. 169-171.

Juyal, P., Mapolelo, M., Yen, A., Rodgers, R. & Allenson, S., Identification of Calcium Naphthenate Deposition in South American Oil Fields, *Energy Fuels* **29** (2015) 2342-2350.

Kauppalehti, Valuutta: USA dollari, http://www.kauppalehti.fi/5/i/porssi/valuutat/valuutta.jsp?curid=USD, Accessed 17 February 2016.

Kimberlin Jr., C. & Judson, M., Removal of metal contaminants from catalytic cracking feed stocks with sulfuric acid, Patent No. US2902430 A, 1959.

Krambeck, F., Lam, C. & Schipper, P., Process for removing metals from crude, Patent No. US4645589 A, 1987.

Kritzer, P., Corrosion in high-temperature and supercritical water and aqueous solutions: a review, *The Journal of Supercritical Fluids* **29** (2004) 1-29.

Kuehne, D., Hawker, L. & Kramer, D., Method for removing calcium from crude oil, Patent No. US6905593 B2, 2005.

Kukes, S., Demetallization of hydrocarbon containing feed streams with phosphorous compounds, Patent No. US4529503 A, 1985.

Kukes, S. & Battiste, D., Demetallization of heavy oils with phosphorous acid, Patent No. US4522702 A, 1985.

Laredo, G., De los Reyes, J., Cano, J.-L. & Castillo, J., Inhibition effects of nitrogen compounds on the hydrodesulfurization of dibenzothiophene, *Applied Catalysis A: General* **207** (2001) 103-112.

Lee, J., Shin, S., Ahn, S., Chun, J., Lee, K., Mun, S., Jeon, S., Na, J. & Nho, N., Separation of solvent and deasphalted oil for solvent deasphalting process, *Fuel Processing Technology* **119** (2014) 204-210.

Leprince, P., *Petroleum Refining, Volume 3 - Conversion Processes*, Editions Technip, 2001, pp. 416-417, 534-536.

Macaud, M., Sévignon, M., Favre-Réguillon, A., Lemaire, M., Schulz, E. & Vrinat, M., Novel Methodology toward Deep Desulfurization of Diesel Feed Based on the Selective Elimination of Nitrogen Compounds, *Industrial and Engineering Chemistry Research* **43** (2004) 7843-7849.

Management Engineering & Production Services, World carbon steel prices, http://www.meps.co.uk/World%20Carbon%20Price.htm, Accessed 18 February 2016.

Mandal, P., Diono, W., Sasaki, M. & Goto, M., Nickel removal from nickel etioporphyrin (Ni-EP) using supercritical water in the absence of catalyst, *Fuel Processing Technology* **104** (2012) 67-72.

Mandal, P., Goto, M. & Sasaki, M., Removal of Nickel and Vanadium from Heavy Oils Using Supercritical Water, *Journal of the Japan Petroleum Institute* **57** (2014) 18-28.

Manning, F. & Thompson, R., *Oilfield Processing Volume Two: Crude Oil*, PennWell Publishing Company, 1995, p. 47.

Marcilly, C., *Acido-Basic Catalysis, Volume 1 - Application to Refining and Petrochemistry*, Editions Technip, 2006, pp. 326-327.

McKetta, J., *Petroleum Processing Handbook*, Marcel Dekker, Inc., 1992, pp. 533-539.

Menon, E., *Transmission Pipeline Calculations and Simulations Manual*, Elsevier, 2015, pp. 156-158.

Moss, D. & Basic, M., *Pressure Vessel Design Manual*, Elsevier, 2013, pp. 186-188.

NFPA, Comparison of NFPA 704 and HazCom 2012 Labels, http://www.nfpa.org/Assets/files/AboutTheCodes/704/NFPA704_HC2012_QCard.pdf, Accessed 13 November 2015.

Northeastern University, NFPA HAZARD RATING SYSTEM, http://www.ehs.neu.edu/laboratory_safety/general_information/nfpa_hazard_rating/, Accessed 13 November 2015.

Panossian, Z., Lira de Almeida, N., Ferreira de Sousa, R., de Souza Pimenta, G. & Bordalo Schmidt Marques, L., Corrosion of carbon steel pipes and tanks by concentrated sulfuric acid: A review, *Corrosion Science* **58** (2012) 1-11.

Parisher, R. & Rhea, R., *Pipe Drafting and Design*, Elsevier, 2012, pp. 121-123.

Parkash, S., *Refining Processes Handbook*, Gulf Professional Publishing, 2003, pp. 16-24, 197-203.

Pauling, L., *General Chemistry*, Dover Publications, 1970, pp. 279-282.

Pohanish, R., *Sittig's Handbook of Toxic and Hazardous Chemicals and Carcinogens*, Elsevier, 2012, pp. 2147-2153.

PotashCorp, Q4 Market Analysis Report, www.potashcorp.com/media/MAR_Q4_2014.pdf, Accessed 26 February 2016.

Powell, R., Removal of metal components from petroleum oils, Patent No. US2778777 A, 1957.

Rand, S., *Significance of Tests for Petroleum Products*, ASTM International, 2010, pp. 48-49.

Riazi, M., *Characterization and Properties of Petroleum Fractions*, ASTM International, 2005, pp. 129-130, 141-142.

Ropital, F., *Corrosion and Degradation of Metallic Materials - Understanding of the Phenomena and Applications in Petroleum and Process Industries*, Editions Technip, 2009, pp. 27-33, 52-55.

Sau, M., Basak, K., Manna, U., Santra, M. & Verma, R., Effects of organic nitrogen compounds on hydrotreating and hydrocracking reactions, *Catalysis Today* **109** (2005) 112-119.

Schobert, H., *Chemistry of Fossil Fuels and Biofuels*, Cambridge University Press, 2013, pp. 267-272.

Seider, W., Seader, J. & Lewin, D., *Product and Process Design Principles: Synthesis, Analysis and Design*, John Wiley and Sons, Inc., 2004, pp. 527-532.

Shekhawat, D., Spivey, J. & Berry, D., *Fuel Cells: Technologies for Fuel Processing*, Elsevier, 2011, pp. 327-329.

Shiraishi, Y., Hirai, T. & Komasawa, I., Photochemical Denitrogenation Processes for Light Oils Effected by a Combination of UV Irradiation and Liquid-Liquid Extraction, *Industrial & Engineering Chemistry Research* **39** (2000) 2826-2836.

Shiraishi, Y., Hirai, T. & Komasawa, I., Photochemical Desulfurization and Denitrogenation Process for Vacuum Gas Oil Using an Organic Two-Phase Extraction System, *Industrial & Engineering Chemistry Research* **40** (2001) 293-303.

Sinnott, R., *Coulson and Richardson's Chemical Engineering Volume 6 - Chemical Engineering Design*, Elsevier, 2005, pp. 815-819.

Speight, J., *The Chemistry and Technology of Petroleum*, Marcel Dekker, Inc., 1999, pp. 235-241.

Srivastava, V., An evaluation of desulfurization technologies for sulfur removal from liquid fuels, *RSC Advances* **2** (2012) 759-783.

Steel Tank Institute/Steel Plate Fabricators Association, Relative Cost Ratio, http://www.steeltank.com/Portals/0/Pressure%20Vessels/SSWseminarOct2012/RelatiRe%20Cost%204%2015%202012.pdf, Accessed 18 March 2016.

Sun, Y., Yang, C., Zhao, H., Shan, H. & Shen, B., Influence of Asphaltene on the Residue Hydrotreating Reaction, *Energy Fuels* **24** (2010) 5008-5011.

Thakore, S. & Bhatt, B., *Introduction to Process Engineering and Design*, Tata McGraw-Hill Publishing Company Limited, 2007, pp. 344-352.

The American Society of Mechanical Engineers, *ASME Boiler & Pressure Vessel Code Section VIII - Rules for Construction of Pressure Vessels*, ASME, 2010, pp. 19-20, 29.

The American Society of Mechanical Engineers, *Pipeline Transportation Systems for Liquids and Slurries*, ASME, 2012, pp. 18-21.

The American Society of Mechanical Engineers, *ASME Boiler & Pressure Vessel Code Section II – Materials*, ASME, 2015.

Toulhoat, H. & Raybaud, P., *Catalysis by Transition Metal Sulphides - From Molecular Theory to Industrial Application*, Editions Technip, 2013, pp. 303-306, 320-321, 618, 680, 703-704.

Towler, G. & Sinnott, R., *Chemical Engineering Design - Principles, Practice and Economics of Plant and Process Design*, 2nd edition, Elsevier, 2013, 1265 p.

Trading Economics, United States Inflation Rate, http://www.tradingeconomics.com/united-states/inflation-cpi, Accessed 22 March 2016.

Walas, S., *Chemical Process Equipment - Selection and Design*, Elsevier, 1990, pp. 663-669.

Yaws, C., *Yaws' Handbook of Properties of the Chemical Elements*, Knovel, 2011.

ZAIN Technologies, Market Pricing: Static Mixers, http://www.zmixtech.com/mixequip/static/Purchase_Static_Mixers.html, Accessed 18 March 2016.

Graph for determining the friction factor in pipes

APPENDIX 1

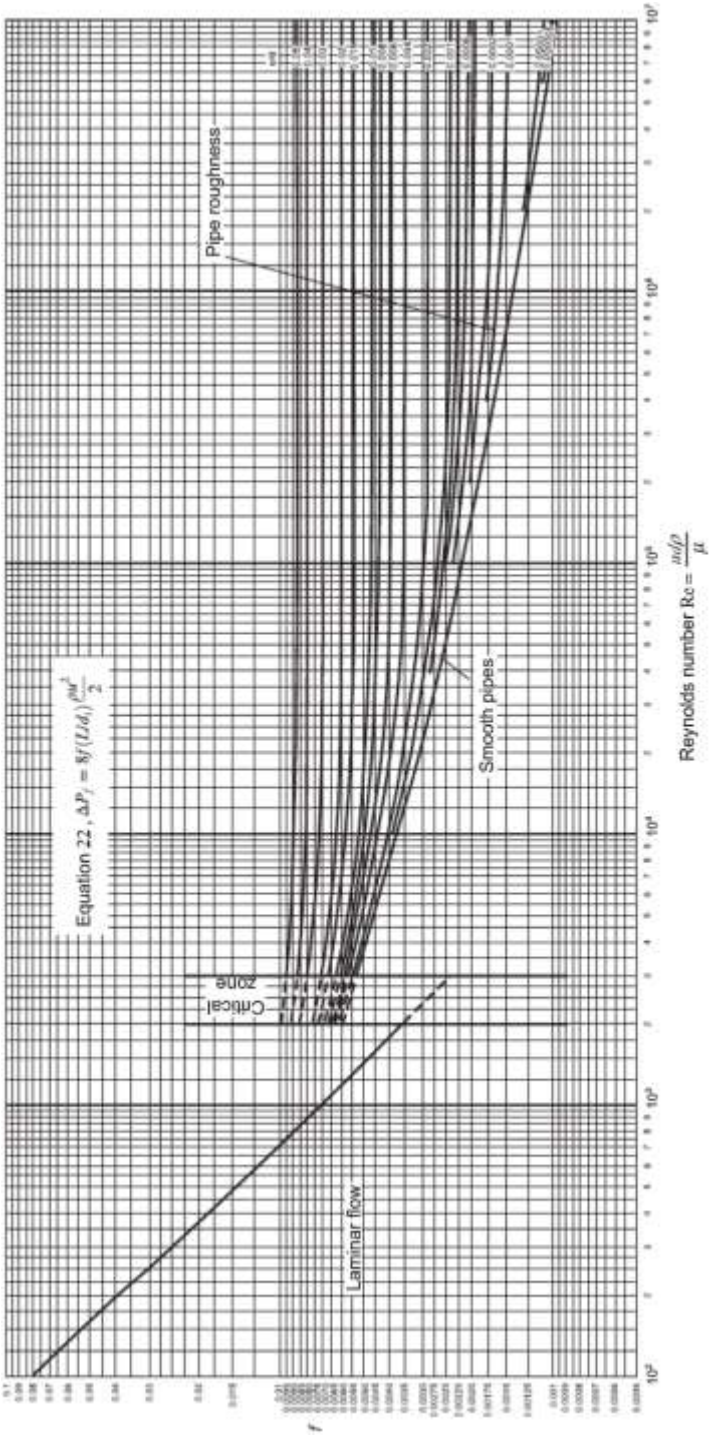

Figure 1. Pipe friction factor in relation to Reynolds number and pipe roughness (Towler & Sinnott, 2013).